END
DATE
FILMED
5-81
DTIC

MICROCOPY RESOLUTION TEST CHART

LEVEL II

(12)

RESPONSE OF A PLAIN AND FILLED ELASTOMER (Solithane 113) TO HIGH STRAIN-RATE COMPRESSION, SHEAR, AND TENSILE LOADING

Technical Report

January 1981

By: Y. M. Gupta and W. J. Murri

Contributor: D. Henley

DTIC
ELECTE
APR 0 8 1981

F

SRI International
333 Ravenswood Avenue
Menlo Park, California 94025
(415) 326-6200
Cable: SRI INTL MPK
TWX: 910-373-1246

81 4 8 003

REPORT DOCUMENTATION PAGE		READ INSTRUCTIONS BEFORE COMPLETING FORM
1. REPORT NUMBER	2. GOVT ACCESSION NO. AD-A097455	3. RECIPIENT'S CATALOG NUMBER
4. TITLE (and Subtitle) RESPONSE OF A PLAIN AND FILLED ELASTOMER (Solithane 113) TO HIGH STRAIN-RATE COMPRESSION, SHEAR, AND TENSION LOADING		5. TYPE OF REPORT & PERIOD COVERED Technical Report. April 1979 - Oct 1980
		6. PERFORMING ORG. REPORT NUMBER SRI Project PYU-7802
7. AUTHOR(s) Y. M. Gupta W. J. Murri		8. CONTRACT OR GRANT NUMBER(s) N00014-78-C-0549
9. PERFORMING ORGANIZATION NAME AND ADDRESS SRI International 333 Ravenswood Avenue Menlo Park, CA 94025		10. PROGRAM ELEMENT, PROJECT, TASK AREA & WORK UNIT NUMBERS 78
11. CONTROLLING OFFICE NAME AND ADDRESS Office of Naval Research Power Program Arlington, VA 22217		12. REPORT DATE Jan 1981
		13. NUMBER OF PAGES 84
14. MONITORING AGENCY NAME & ADDRESS(if different from Controlling Office)		15. SECURITY CLASS (of this report) Unclassified
		15a. DECLASSIFICATION/DOWNGRADING SCHEDULE

16. DISTRIBUTION STATEMENT (of this Report)

Approved for public release, distribution unlimited

17. DISTRIBUTION STATEMENT (of the abstract entered in Block 20, if different from Report)

18. SUPPLEMENTARY NOTES

19. KEY WORDS (Continue on reverse side if necessary and identify by block number)

Mechanical Response, Elastomer, High Strain Rate, Compression, Shear, Tension, Stress Waves

20. ABSTRACT (Continue on reverse side if necessary and identify by block number)

To quantify the high strain-rate mechanical response of plain Solithane, compression, shear, and tension experiments were performed under impact loading (microsecond time scales). Compression and tension measurements were carried out for filled Solithane containing 56.5 wt% of glass beads. The results show that the compression response (uniaxial strain) of plain Solithane is dominated by the mean stress-volume relation. The bulk modulus under impact loading is considerably higher than that determined from static

DD FORM 1473 EDITION OF 1 NOV 65 IS OBSOLETE
1 JAN 73

Abstract (concluded)

measurements in the glassy state. The filled Solithane compression response
can be approximated by a simple mixture theory using the Hugoniots of plain
Solithane and glass..

Shear wave measurements in the plain Solithane were used to determine the
shear modulus and the shear stress-strain response at several shock compress-
ions. The shear modulus varied between 3 and 9 kbar for compressive stresses
ranging between 2 and 14 kbar. With increasing compression, the dynamic shear
modulus increases sharply in contrast to quasi-static measurements under
pressure. The dynamic shear stress-strain curves show a decreasing modulus
with increasing strain and suggest an elastic-plastic response with yield
strength increasing from 0.12 to 0.25 kbar with increasing pressure for the
compressive stress range investigated. This direct determination of the shear
response will be very valuable for development of constitutive models because
this information cannot be obtained from compression data.

Tension experiments on plain and filled Solithane show elastic-brittle
fracture response for both materials. However, the threshold between no
damage and full spall is considerably sharper for the filled Solithane. The
sharper threshold is caused by the rapid linking of closely spaced cracks
nucleated at the filler-matrix interface. The tensile damage is very localized
and the location can be predicted by simple wave interactions. Two experi-
mental methods were attempted to quantify the fracture response on the micro-
second time scales and to measure the fracture damage in the recovered
specimens. These measurements have given encouraging results, but more work
is needed before they can be used successfully. Because of a lack of quanti-
tative measurements in previous studies, we will pursue these measurements
further in future work.

CONTENTS

iii

LIST OF FIGURES

LIST OF TABLES

PREFACE

Section 1

INTRODUCTION

1.1 Motivation

In recent years, high strain-rate deformation and fracture of energetic materials (propellants and explosives) have received increased attention.[1-7] This interest has been prompted by the need to better understand the role of mechanical deformation in phenomena like DDT[3,8] (deflagration to detonation transition) and impact initiation.[1,2,4,6] In shock initiation problems, the creation of hot spots is postulated as the mechanism for starting the chemical reaction. Although the micromechanism(s) and the material properties responsible for creating the hot spots have not been precisely identified, the importance of inelastic deformation and fracture processes in creating hot spots is widely accepted.[6] A better quantitative understanding of the inelastic processes can be achieved by determining the material response under different, well-defined loading conditions.

Heterogeneous energetic materials have an additional variable that must be considered: the properties of the elastomer or binder. Although the binder is generally an inert material, its mechanical properties can and probably do influence the response of the composite material. For example, the shear deformation of the binder may govern the threshold for localized shear deformation whereas the tensile properties of the binder may govern the dewetting behavior and linking up of cracks through the matrix. Therefore, it would be desirable to determine the binder properties (mechanical) that influence the dynamic deformation of the composite material.

The study of mechanical deformation of energetic materials not only is a complex theoretical problem (combined mechanical-thermal-chemical interaction), but it also poses special experimental difficulties. An idealized approach[9] to circumvent these difficulties is to study mechanically similar inert materials, such as filled elastomers. Although these

1

model systems cannot simulate many aspects of the energetic material response (related to chemical energy release), they can provide several important pieces of information: (1) the type of experiments that are optimal in defining the mechanical response, (2) the microscopic and continuum processes that dominate the mechanical response, and (3) the type of continuum material models needed to incorporate the important microscopic processes. If success can be achieved in describing the continuum response of model systems, then work can be extended to energetic materials of interest.

This technical report describes the work done to date in an ongoing research effort to quantify the high strain-rate mechanical response of a plain and filled elastomer. A brief technical background and the scope of our work is presented next. Our discussion focuses on the high strain-rate response--the main theme of our work.[10]

1.2 Background and Objectives

Studies of high strain-rate deformation of energetic materials can be classified in two main categories:[11] (1) plate impact experiments and analysis to better correlate the hydrodynamics with the liberation of chemical energy, and (2) empirical test results (e.g., drop test, friction test, gap test) to evaluate performance for specific applications. It is, however, difficult to analyze these data to determine and model the high strain-rate mechanical response. In many of the above-cited tests, it is difficult to separate the effects of different load types: compression, shear, and tension. Even for nonenergetic polymers, there are few studies detailing the mechanical response at high rates of loading. In contrast, mechanical deformation of polymers (including elastomers) at low strain-rates has been extensively studied.[12,13]

The most thorough investigation of the constitutive response of a polymer at high strain rates is the shock work (uniaxial strain) on PMMA performed at Sandia Laboratories. A comprehensive account of the Sandia work is given in Reference 14. Two important results of this work are as follows. First, below 8-kbar compressive stress, the PMMA can be modeled

as a nonlinear viscoelastic solid (or even a nonlinear elastic solid to a good approximation). Good correlation was found with ultrasonic wave velocity and attenuation measurements. Second, above 8 kbar, the experimental results suggested an inelastic response accompanied by dilatancy. The exact nature of the inelastic deformation was not established in these studies. The results of two more recent studies on PMMA are discussed later in this section.

The tensile response of polymers under impact loading has been investigated in studies at SRI.[15-17] In one study,[15] tensile fracture due to stress wave interaction was examined in a polycarbonate. Penny-shaped tensile cracks were observed in the impacted specimens. The observed crack distributions and damage locations were quantitatively simulated using an elastic-brittle fracture model. The brittle fracture response was represented by a nucleation and growth (NAG) model in agreement with the microstructural observations. Studies on filled elastomers (propellants[16] and composite explosives[17]) have been less successful in quantifying the tensile damage and the fracture process. Although the use of the nucleation and growth model seems appropriate and desirable,[16] it is difficult to determine the material parameters and to quantitatively compare calculations and experiments, as was done for the polycarbonate.[15]

Unlike compression and tension results, there existed no prior material property studies on the high strain-rate shear properties of polymers,* and we can only conjecture about the dynamic shear response (summarized below) based on quasi-static studies.[19]

Based on the past high strain-rate and quasi-static studies, the following features are expected to be important in describing the response of elastomers: (1) strong dependence of modulus on confining pressure and loading rates, (2) strong dependence of material strength on confining pressure and loading rates, (3) inelastic shear deformation, (4) role of voids and inclusions in tensile cracking, (5) stress relaxation due to tensile cracking and possibly shear failure, and (6) influence of

---

*This statement ignores work in Reference 18 that was started concurrently with the present work.

3

temperature on mechanical response. These features show that the development of a general constitutive model for elastomers is a difficult and challenging problem. Furthermore, sufficient data do not exist to satisfactorily undertake such a development at present. Hence, there is a need for experimental results under different, well-defined dynamic loading conditions to quantify the above-cited material properties.

In the present study we have chosen to determine separately the compression, shear, and tensile response of elastomers by controlled impact experiments. We have examined both plain and filled elastomers to better understand the role of binder properties on the response of the filled material. An important feature of our work is the direct measurement of the dynamic shear response, since no experimental data exist for this area. The importance of shear measurements was demonstrated in a recent study on PMMA.[18] The measurements of compression and shear velocity in the shocked state demonstrated the presence of strain-softening with increased compression beyond 8-kbar stress. This phenomenon is most likely related to the temperature rise recently reported in PMMA.[20]

The scope of the present work has been primarily experimental with the emphasis on development of experimental techniques, obtaining reliable measurements, and interpreting these data. An example of this emphasis is our attempt to quantify the tensile fracture process and the observed damage. Previous studies on similar materials have not addressed these issues.[16,17]

Section 2

EXPERIMENTAL METHOD

This section describes the experimental techniques designed and developed to obtain the high strain-rate material response under compression, shear and tension. The discussion emphasizes methods that were specifically developed for the present work, including experimental assembly for a thermally cured elastomer. Before discussing the impact experiments, we describe the particular elastomer used in our work.

2.1 Material Selection and Characterization

In conjunction with the other ONR investigators, we selected Solithane 113 for our study. This is the trade name for a polyurethane elastomer, manufactured by the Thiokol Chemical Corporation, that is furnished as a urethane resin and a catalyst. Past work at Caltech has characterized the static mechanical properties for various compositions of the resin and catalyst.[21] We exclusively used the 50/50 volume composition. Initially, it was decided that all specimens would be cast at one location (Caltech). However, we found this arrangement to be impractical and set up our own casting facility to reproduce the mixing and casting procedures at Caltech. In addition, we refurbished an existing propellant mixer to vacuum-mix and cast filled Solithane specimens. Spherical glass beads were used as filler material and the filled specimens contained 56.5 wt% of glass beads.[22] More details of the casting method are presented in Appendix A. Some properties of the unfilled and filled Solithane 113 are shown in Table I. Our casting techniques gave reproducible and void-free specimens. The measured density of the filled specimens was within 1 percent of the theoretical density. After a thin layer ($\sim$ 1 mm) was removed from the ends of our 5-cm-long cylindrical samples, the density variations were less than 2 percent through the sample length.

Table I

PROPERTIES OF PLAIN AND FILLED SOLITHANE 113

Resin/Curing Agent Composition   50/50

Density of plain Solithane 1.04 g/cm^3

Wt. fraction of glass beads   56.5%

Diameter of glass beads   40–80 μm

Density of glass beads 2.42 g/cm^3

Density of filled Solithane 1.53 g/cm^3

Static and acoustic experiments were also conducted because of their usefulness to the constitutive model development.* The static data are useful in ascertaining rate effects by comparison with dynamic data, in providing information about the behavior in the glass transition region, and in studying the effect of loading paths. The acoustic data at ambient and high pressures can provide bulk and shear moduli at frequencies (MHz) comparable to the impact data.

The results from the quasi-static experiments were not successful. Despite several repetitions, of the experiments, the data were inconsistent and incorrectly showed material anisotropy. The extremely compliant nature of the material did not permit accurate transverse strain measurements. Because this static effort was of secondary interest, we discontinued this work. Instead, we decided to use the hydrostatic data of Questad et al.[24] for comparisons with the high strain rate data (Section 4).

The acoustic measurements provided longitudinal wave velocity measurements as a function of confining pressure, and these are shown in Table II. To obtain these data, length corrections were made using the axial strain measurements in the hydrostatic experiments. Although the acoustic measurements are expected to be correct, independent confirmation would be desirable. The shear wave velocity measurements were not successful. Our discussions with other workers[25] conducting similar measurements and our examination of data in propellants[26] indicate that the inability to make shear measurements in such materials is a common problem. Because of the potential usefulness of the shear wave data and the quasi-static triaxial data in material characterization, these experiments should be attempted in the future with improved techniques.

_____

*This work was performed by Terra-Tek Inc.[23] under subcontract.

Table II

LONGITUDINAL WAVE VELOCITIES (mm/μs)[*]

	CP[†]	CP	CP	CP
	0	1.38	2.76	4.14
Plain Solithane	1.72	2.14	2.46	2.74
Filled Solithane	1.85	2.33	2.69	2.94

---

[*]See remarks about accuracy in the text.

[†]Confining pressure (kbar).

8

2.2 Impact Experiments

Plate impact experiments, the main theme of our work, were conducted on both plain and filled Solithane. Figure 2.1 shows a schematic view of the impact of two parallel plates. Upon impact, stress waves propagate in the flyer and specimen plates. Restricting attention to the center of the plate (for large lateral dimensions), variations with respect to only one spatial coordinate, X_1, need to be considered in the governing equations. When the normal to the plates is not parallel to the projectile motion axis ($X_1^{\prime}$), as shown in Figure 2.1, both compressive and shear motions (along X_1 and X_2 axes) are produced at the impacting surfaces. These jumps in compressive and shear motions are propagated in the specimen interior with the respective wave speeds.

The experimental data consisted of compression (u_1) and shear (u_2) particle velocity measurements at several depths in the specimen interior.[27] The particle velocities were obtained from a measurement of the voltage induced by the motion of a known length of conductor (wire or foil gages) in a constant magnetic field (Faraday's Law for moving circuits):

$$E = \vec{\ell} \cdot (\vec{u} \times \vec{B}) \tag{1}$$

where E is the emf, $\vec{\ell}$ is the length vector along the gage, $\vec{u}$ is the particle velocity, and $\vec{B}$ is the magnetic field. By appropriate orientation of the $\vec{B}$ field, either u_1 or u_2 can be obtained.

A detailed account of the experimental facility used to produce and measure one-dimensional compression and shear waves is given in Reference 28. A discussion of the theoretical aspects of compression and shear wave propagation is given in Reference 29, and the governing equations are summarized and discussed in Appendix B. The following subsections describe the specific techniques used to measure compression, shear, and tensile response of the Solithane.
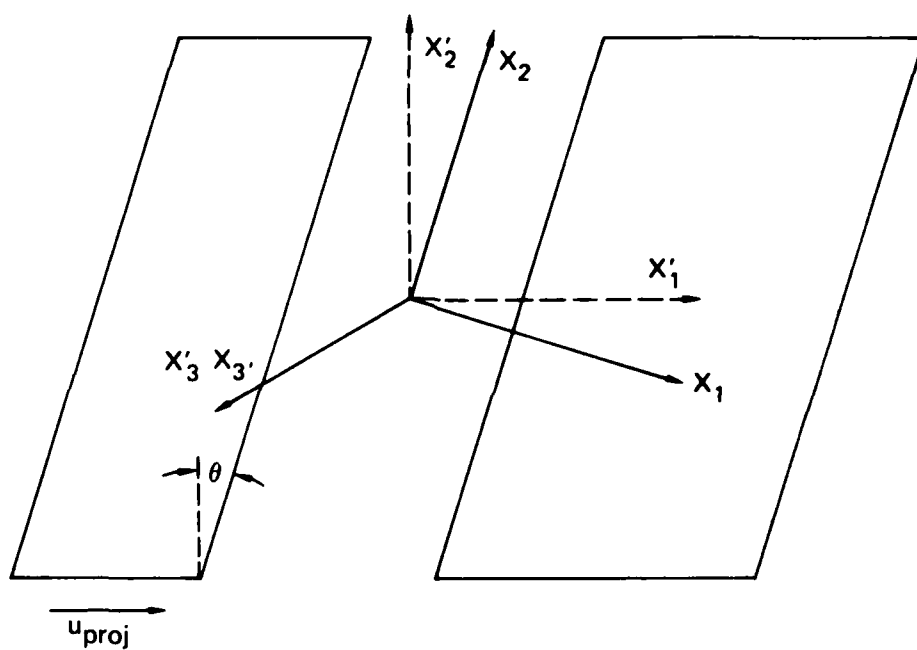
MA-5746-2C

FIGURE 2.1   SCHEMATIC VIEW OF EXPERIMENTAL TECHNIQUE TO PRODUCE
COMPRESSION AND SHEAR WAVES

2.2.1 Compression Response

If the angle θ in Figure 2.1 is set to zero, the material response is for a plane compression wave (uniaxial strain). For $\theta \neq 0$, there is superposed shear deformation. However, as discussed in Appendix B, the measurement of purely longitudinal motion, u_1 (t), is sufficient to determine the compressive stress-volume (σ_x - V) response even under combined loading. In all of the compression response experiments, the magnetic field vector was aligned to measure only u_1 (t).

In most compression experiments, three or four particle velocity gages were cast in the specimen, as shown in Figure 2.2(a). A representative photograph of a completed specimen assembly with two gages is shown in Figure 2.2(b). The elevated temperatures for curing the Solithane and the subsequent specimen shrinkage required special assembly procedures (see Appendix A). The gage configuration shown in Figure 2.2(a) was developed after several preliminary attempts. In this configuration, the active gage elements were made from 0.05-mm-diameter copper wires and were 7 to 10 mm in length. These wires were carefully soldered to 0.25-mm-diameter copper posts that were brought out through the back of the specimen. Although foil gages are generally preferable in impact experiments, the necessity of bringing the leads through the back and minimizing the surface area for thermal strains required the use of wire gages.

The specimen containing the wire gages was cast in a target ring for the impact experiments. Because of the compliant nature of the Solithane, the target ring and the specimen could not be lapped. This difficulty had two main effects: Our impact alignments (between 1 to 2 mrads) were not as good as the usual shock wave experiments, and particle velocity gages and impact alignment strips could not be vapor-deposited on the sample surface. The first effect is not very important for a material like Solithane. The second effect was circumvented by measuring particle velocity close to the impact surface (within 0.22 mm) and by using copper foils (0.013-mm-thick) to measure impact alignment.

11

Gages

2.54 cm

6.35 cm

Solithane

(a)

(b)
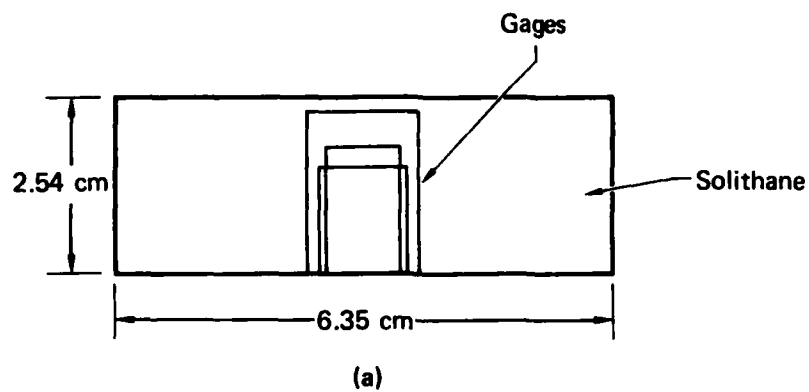
JP-7802-1

FIGURE 2.2 TARGET ASSEMBLY FOR GAGE EXPERIMENTS

(a) Schematic side view of the gages in a Solithane block;
(b) Photograph of the target assembly with two gages
at depths of 1 and 2 mm.

12

The voltage signals from the gages were recorded using the usual methods. To obtain good time correlations between gages, we recorded successive gages on a series of fast dual-beam oscilloscopes (Tektronix 7844). This procedure permitted an accurate determination of wave velocities and an improved analysis of the experimental data.

2.2.2 Shear Response

The measurement of shear response requires that the angle in Figure 2.1 be $\theta \neq 0$. For measuring the shear particle velocity, $u_2(t)$, the magnetic field must be appropriately aligned so that the voltage in Eq. (1) has only u_2 contribution. Despite good field alignment, shear particle velocity measurements are not as accurate as longitudinal data. (This feature will become apparent in Section 3.) The large relative magnitude of the faster traveling longitudinal wave coupled with small errors in magnetic field alignment and impact tilt produce a small perturbation that occurs before shear wave arrival.[28] The large relative magnitude of the compression wave is a consequence of material behavior, and merely increasing θ does not produce larger shear deformation in the specimen.

The experimental assembly for shear wave experiments was identical to that for the compression experiments. However, the gage locations were different for the two sets of experiments. After some initial experiments, we discovered the relatively slow velocity of shear waves in the Solithane. (These low values are probably characteristic of most elastomers and may explain the difficulty in acoustic measurements.) In all subsequent experiments, the gages were located at depths of 0.25, 1.0, and 2.0 mm into the specimen. These small values are required to preserve the one-dimensionality of the experimental measurements. Unfortunately, the small separation between gages results in larger errors in wave velocities.

The shear particle velocity data were also used to determine the dynamic shear stress-strain response in Section 4.

13

2.2.3 Tensile Response

Two types of tensile loading experiments were performed: those in which the samples were recovered for postimpact examination, and those in which particle velocity gages were used to actively monitor the tensile fracture by measuring the recompression signal due to fracture. As it turned out, we were also able to recover most of the specimens in the second type of experiment (termed pull-back measurements). The complementary nature of these two experiments will become clear in the subsequent discussion.

The formation of tension is shown in Figure 2.3(a). Upon impact, compression waves propagate in the flyer and specimen plates. Tension is produced by the intersection of the rarefaction waves reflected from the free surfaces. The position where tension first forms, as well as the magnitude and duration of the tensile pulse, are governed by the impact velocity and thicknesses of the impacting plates. If the tensile pulse results in material damage, then the magnitude and the duration of the pulse are subsequently changed by the growing damage.

Because most materials cannot sustain large tensile stresses and strains, an elastic wave analysis can often be used to design the experiments. Analysis of the results, however, is more difficult because of two main factors: stress relaxation due to damage, and nonlinear elastic moduli. A rigorous analysis requires the use of computational models.[30]

2.3 Recovery Experiments

The experimental arrangement for recovery experiments is shown in Figure 2.3(b). The sample of interest (termed a puck) is surrounded by similar material. Upon impact, the specimen puck is pushed out and collected in the recovery chamber for subsequent microstructural examination. The purpose of the surrounding material is to mitigate the effects of edge waves. Although the edge waves cannot be completely eliminated, they can be minimized by proper experimental design. The steel ring and the honeycomb are used to decelerate the projectile.
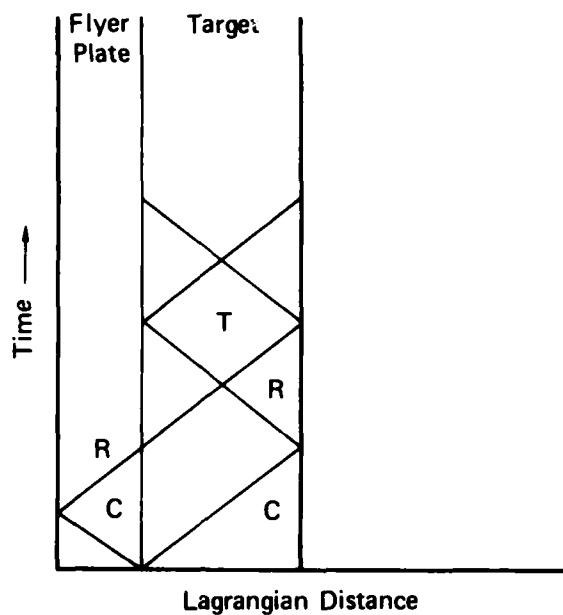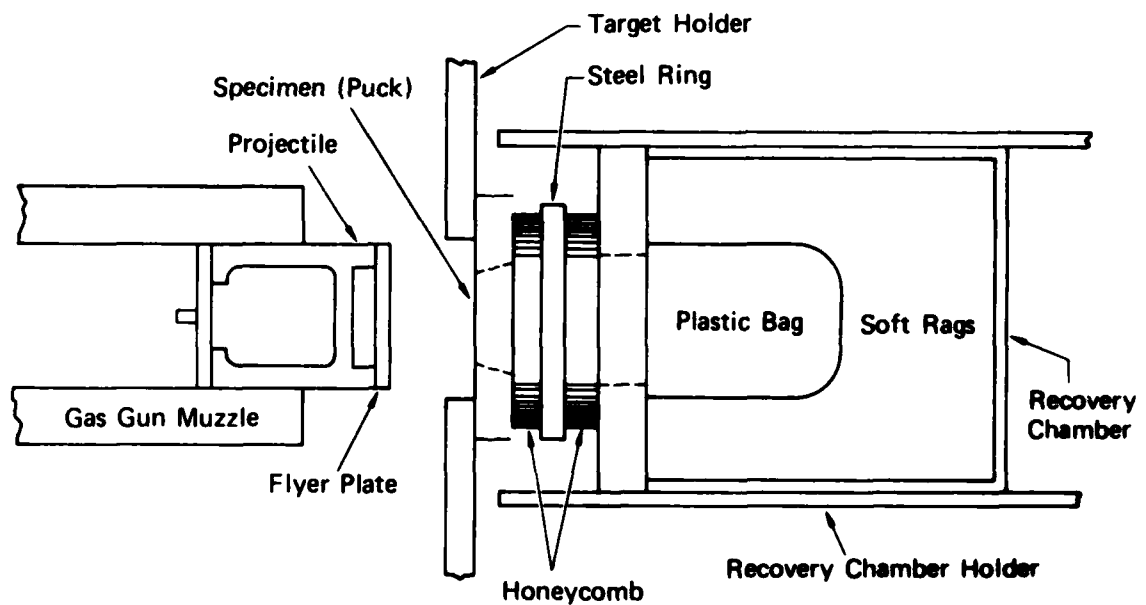
FIGURE 2.3   DETAILS OF TENSION EXPERIMENTS

(a) Formation of tensile pulse from interaction of two rarefactions;
(b) Arrangement for soft recovery of target.

The target assembly shown in Figure 2.3(b) was cast in two steps. First, material surrounding the puck was cast with an aluminum puck. Upon curing, the aluminum puck was removed and the central specimen puck was cast using a mold release. After the central puck was cured, it was pushed out to ensure that it would come out in the experiment. Subsequently, the specimen puck was pushed back in and the surfaces were ground to ensure a planar impact.

The effect of superposed shear on tensile fracture damage can be examined using the experimental arrangement shown in Figure 2.3(b) except that the flyer and specimen plates are inclined at an angle θ to the projectile motion axis (as shown in Figure 2.1). Although the effect of shear on specimen damage has been previously observed in a composite explosive,[17] we have not examined this effect in detail in our present work. A few preliminary experiments are discussed in Section 3.

Once the specimens have been recovered, damage must be measured and quantified. Past work on tensile fracture has consisted of microstructural examination in sectioned specimens using optical microscopy.[15,30] For many metals and glassy polymers this technique has provided quantitative estimates of crack size distributions for various levels of damage. In the studies on elastomers, the microscopic examinations provided useful information about the damage phenomenology. However, as discussed in Section 3, it is difficult to quantify these results. We had anticipated this difficulty based on our previous work in propellants[16] and explosives[17] and performed the following measurements to quantify the damage.

Of particular interest for filled elastomers (propellant-like materials) are the measurements of surface area and the volume porosity generated by the fracture damage. These results not only quantify the various levels of damage, but also will provide a check for our future constitutive modeling effort. The surface area measurements were made using the BET (named after Brunauer, Emmett, and Teller) gas adsorption method.[31] In the BET method, measurements are made of the amount of gas adsorbed at a given pressure by the surface of a specimen. The surface area of the specimen can then be calculated from these measurements. The volume porosity measurements were made using a mercury porosimeter. Both of these techniques are standard in materials characterization and details may be seen in Reference 31.

2.4 Pull-back Signal Measurements

The preceding discussion has focused on postimpact observations. Although such data are very useful, it is difficult to completely eliminate late-time effects and experimental artifacts due to the recovery techniques, and to quantify the damage. To minimize these difficulties, we supplemented the recovery experiments with the pull-back signal measurements. These experiments have been performed previously in metals[32] and geologic solids.[33] However, there are some unique problems in studying elastomers, as discussed later.

Figure 2.4 shows the distance-time plot and the corresponding free surface particle velocity-time plot for an idealized experiment.* At time t_1, the compression wave reaches the back surface and produces a velocity shown by the point B. The reflected waves from the specimen and flyer plates intersect to produce tension in the specimen. If the tensile pulse magnitude is less than the tensile strength, no damage occurs and the free surface particle velocity drops to zero at t_2. If the tensile pulse exceeds the tensile strength and the specimen is a perfect brittle solid (zero strain to failure), then the fracture is instantaneous. CE is a measure of the tensile strength, and for a perfectly brittle material the time separation EF = 0. The increase in particle velocity at time F is the recompression signal due to the spall in the specimen--hence, the term pull-back measurement. For most materials the more rounded signal shown in the middle in Figure 2.4(b) is typical.[32,33]

We can briefly summarize the main features of the pull-back signal measurements as follows: (1) the particle velocity drop CG is a measure of the dynamic tensile strength, (2) the curvature in the profile CG is a consequence of the nonlinear elastic modulus (for elastomers, this is important), (3) the shape of the profile GH provides the information about fracture kinetics, and (4) the particle velocity drop CH is a measure of the energy dissipated in the fracture process and the extent of spall.

---

*The gage, although very close to the free surface, is not at the free surface.
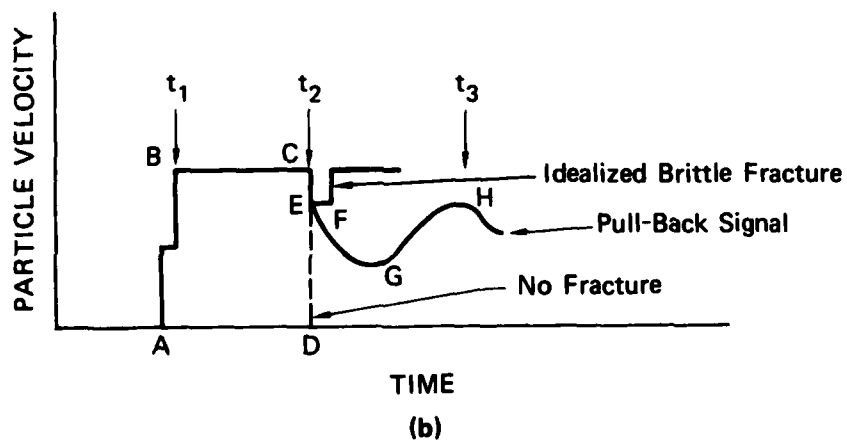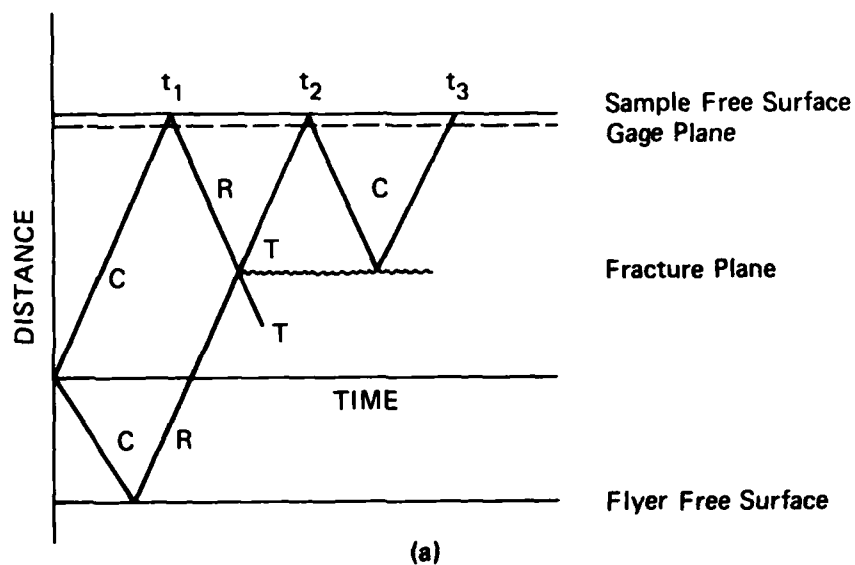
FIGURE 2.4   DETAILS OF PULL-BACK SIGNAL MEASUREMENTS

(a) Distance-time plot; (b) Particle velocity profile occurring at the gage plane. For a perfectly brittle solid, the time separation EF = 0.

18

For the study of high mechanical impedance materials, the sample is backed by a low impedance buffer (typically, a polymer-like PMMA) and the particle velocity is measured at the sample-buffer interface or in the buffer material.* With a very low impedance material like Solithane, this procedure is not possible. Our initial attempts to measure free surface velocities using particle velocity gages bonded to the rear surface of the sample were unsuccessful.[34] Subsequently, we altered our technique and cast gages very close to the rear surface (within 0.5 mm). This technique, though difficult to implement, is conceptually valid and has provided data. However, the gage lead breakage continues to be a problem and we are working on solving this problem. (Unlike our compression and shear measurements, the gage leads must be brought out through the side and this causes lead stretching at late times.) Because of the promising results achieved to date and the potential to quantify the fracture process, we will attempt to further refine this method in future work.

---

*In metals, the free surface velocity can be directly measured.

Section 3

EXPERIMENTAL RESULTS

The majority of the data from the impact experiments are on plain Solithane. The experiments on filled Solithane consisted of two compression experiments and several tension recovery experiments. The main purpose of the filled Solithane experiments was to allow a preliminary comparison with the plain Solithane results, particularly the tension response. Future work will concentrate on filled Solithane specimens.

3.1 Compression Wave Measurements

Table III summarizes the experiments in which we measured the compression wave profiles. A representative set of data, taken from experiment 3 (80-2-33), is shown in Figure 3.1. The gage locations were 0, 1.04, 3.53, and 6.3 mm from the impact surface. A nearly flat-topped wave (peak stress of 6.1 kbar) followed by a dispersive relief wave propagates through the sample. The small overshoot in the initial jump is an experimental artifact caused by the use of wire gages. The unloading wave amplitude does not drop to zero because the impactor (PMMA) has a higher mechanical impedance than the Solithane. The useful recording time in these experiments ranges between 6-7 μs after impact. The compression and release wave velocities were obtained from the onset of the compression and the release portions of the wave profiles. Because the release waves propagate in the shocked region, the data in Table III have to be corrected for compression.

The records shown in Figure 3.1 are typical of most of the compression data and are similar to shock wave data in PMMA.[35] These records are analyzed in Section 4 to provide the stress-volume relations. Experiments 2 (79-2-9) and 3 (80-2-33) were performed at nearly the same impact velocity. Shot 2 was performed on one of our earlier specimens, whereas shot 3 was performed more than a year later. The compression wave

21

Table III

SUMMARY OF COMPRESSION EXPERIMENTS

Specimen	Experiment No.	Proj. Vel. (mm/μs)	Impactor Material	Angle θ	Particle Vel.[b] (mm/μs)	Wave Velocities (mm/μs) Compression[c]	Release[c]
	1. (80-2-34)	0.165	PMMA	0°	0.098 ± 0.005	1.7[d]	2.09[d]
	2. (79-2-9)[a]	0.4	PMMA	0°	0.22 ± 0.005	2.26	2.7
Plain Solithane	3. (80-2-33)	0.411	PMMA	0°	0.233 ± 0.007	2.34	3.2
	4. (80-2-35)	0.497	Granite	0°	0.394 ± 0.008	2.71	3.93
	5. (80-2-45)[a]	0.424	PMMA	10°	0.242 ± 0.01	--	--
Filled Solithane	6. (79-2-41)	0.143	F. Solithane	0°	$0.081^{e} \pm 0.001$	2.03	2.44
	7. (79-2-42)	0.329	F. Solithane	0°	$0.18^{e} \pm 0.01$	2.33	3.10

[a] See remarks in text about these experiments.

[b] These values reflect the average peak value and scatter for all gages in that experiment.

[c] These values have not been corrected for compression.

[d] These measurements have lower precision (6-8 percent) than the other experiments (2-4 percent).

[e] These amplitudes are greater than half the impact velocity. See text for explanation of error.
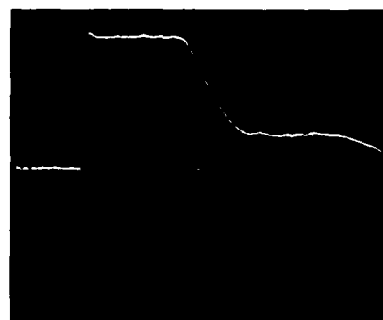
JP-7802-4

FIGURE 3.1   COMPRESSIVE WAVE PROFILES (PEAK STRESS = 6.1 kbar)

The gage records are from Experiment 80-2-33. Gage locations
are 0, 1.04, 3.53, and 6.3 mm.

23

velocities vary by about 3.5 percent and the release wave velocities vary by about 15 percent. The large difference in the release wave velocities is not understood.

Experiment 5 (80-2-45) was performed to measure the compression wave response under combined compression and shear loading. Unfortunately, the gages broke about 1 μs after the first jump and the records were quite noisy. The gage breaking in experiment 5 is not linked to the shear deformation because a similar assembly was used in the shear wave measurements. Although the overall records are similar to the other data, the accuracy in compression wave velocity was poor. In a compression-shear experiment, all of the gages beyond the first gage experience only uniaxial strain compression for most of the pulse duration; this is due to the extremely low shear wave velocity. Hence, even under combined compression and shear wave experiments, the compression data reflect the uniaxial response.

The particle velocity amplitudes in Table III indicate a precision of 3 to 5 percent in our plain Solithane experiments. This number is somewhat higher than the 2 to 3 percent precision we have normally observed in our data on other materials like PMMA. The larger discrepancy is attributed to the error in casting the gages and possible changes in gage length resulting from strains caused by curing.

The filled Solithane shots had two main purposes: to provide longitudinal stress-strain data for interpreting the tension experiments and to ensure that our gage assembly was satisfactory. Three shots were fired with the filled Solithane specimens, two of which are reported in Table III. The third shot, at a stress of 10 kbar, showed a precursor ahead of the main wave. Unfortunately, lead artifacts obscured accurate measurements.

Unlike the unfilled Solithane specimens, the gage leads in the filled specimens came out of the side. We believe the side leads cause the amplitude errors and experimental artifacts seen at the higher stresses. Further work on filled Solithane will be done with leads coming through the back.

In the two experiments reported in Table III, the records appeared similar to those for the unfilled data except that the wave velocities were higher, as expected for a stiffer material.

In summary, the compression wave profiles are similar to those observed in a glassy polymer like PMMA. This is not surprising for two reasons: The Solithane is expected to respond in a glassy manner at these stresses and loading rates, and the material response is dominated by the mean stress-volume response. However, there are important strength differences in the PMMA and Solithane.

3.2 Shear Wave Measurements

A total of nine shear wave experiments were performed, six of which are summarized in Table IV. The other three experiments were preliminary shots designed to obtimize the experimental design and assembly. Data from experiments 1 (80-2-48), 2 (80-2-46), and 5 (80-2-66) are shown in Figures 3.2 through 3.4, respectively. The negative voltage due to the shear wave is a consequence of the magnetic field orientation. The peak compressive stress ranged from 2.1 kbar (80-2-48) to 14.3 kbar (80-2-66).

In contrast to compression wave experiments, the gages for shear wave measurements were located very close to the impact surface: 0.25, 1.0, and 2.0 mm from the impact surface. The closeness to the impact surface is required by the slow shear wave velocity. Figure 3.2 shows the shear wave profiles at a compressive stress of 2.1 kbar. A small perturbation due to the longitudinal wave can be seen at early times. This is followed by the main gage signal due to the shear wave. Although the wave is not attenuating, it is quite dispersive. In fact, at gage 3. the rise time is so large that only the initial portion of the shear wave can be seen. The difference in the magnitude of the perturbation, resulting from the longitudinal wave, between gages 2 and 3 is quite marked and reflects the limitation of gage fabrication and casting techniques.

Table IV

SUMMARY OF SHEAR EXPERIMENTS[a]

Experiment No.	Proj. Vel. (mm/μs)	Impactor[b] Material	Angle θ	Shear Wave Velocity[c] (mm/μs)
1 (80-2-48)	0.175	PMMA	15°	0.59
2 (80-2-46)	0.422	PMMA	10°	0.68
3 (80-2-65)	0.429	PMMA	15°	0.61
4 (80-2-51)	0.502	Granite	5°	0.95
5 (80-2-66)	0.576	Granite	5°	0.93
6 (80-2-59)[d]	0.5	Granite	0°	--

[a]All experiments were performed with plain Solithane.

[b]The properties of the PMMA and Granite are given in References 35 and 36, respectively.

[c]These velocities have not been corrected for compression.

[d]This experiment was designed as a check on the experimental method; because θ = 0°, no shear wave signal was expected.
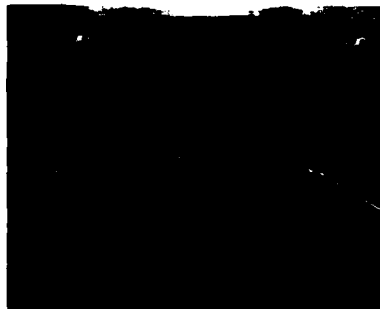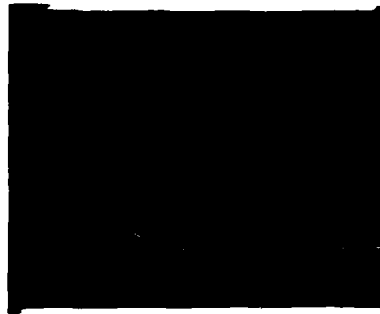
JP-7802-5

FIGURE 3.2   SHEAR WAVE PROFILES (COMPRESSIVE STRESS = 2.1 kbar)

The gage records are from Experiment 80-2-48. Gage locations
are 0.25, 1.0, and 2.0 mm. The large dispersion did not permit
complete recording of the wave at the last gage.

27
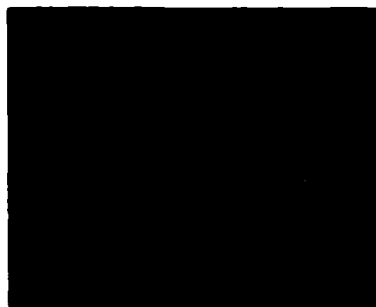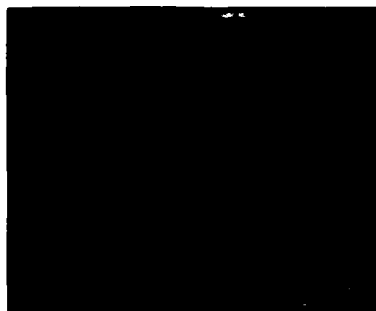
JP-7802-6

FIGURE 3.3 SHEAR WAVE PROFILES (COMPRESSIVE STRESS = 6.1 kbar)

The gage records are from Experiment 80-2-46. Gage locations are 0.25, 1.0, and 2.0 mm. The last gage broke before shear wave arrival.
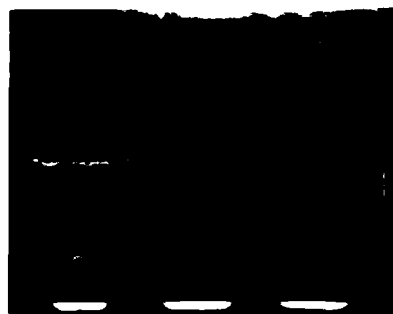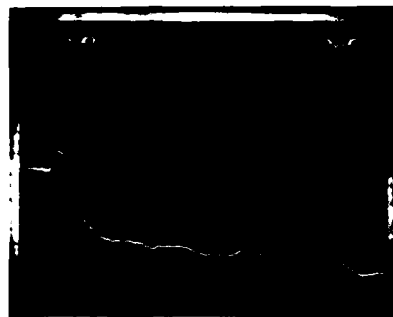
JP-7802-7

FIGURE 3.4   SHEAR WAVE PROFILES (COMPRESSIVE STRESS = 14.3 kbar)

The gage records are from Experiment 80-2-66. Gage locations
are 0.25, 1.0, and 2.0 mm; the last record was delayed by 1 μs.

29

At a compressive stress of 6.1 kbar (Figure 3.3), the shear wave rise time is smaller, but the peak amplitude is attenuating. The record from gage 3 suggests that the gage broke.

At a compressive stress of 14.3 kbar (Figure 3.4), the rise times are considerably smaller. However, the wave profiles are both dispersive and attenuating. The perturbation due to the longitudinal wave is quite small for gages 2 and 3. Note, the gage 3 record shown in Figure 3.4 was delayed by 1 μs.

Data from experiment 4 (80-2-51) at a compressive stress of 12.0 kbar are similar to the data in Figure 3.4. Data from experiment 3 (80-2-65), which was designed to duplicate experiment 2, showed considerably smaller amplitude at all the gages. Evidently the shear amplitude was not completely coupled into the specimen.

The wave velocities shown in Table IV are determined from the onset of the shear motion. The precision of the shear wave velocity measurements is approximately 10 percent and is lower than that of the compression wave velocities. The reasons for the lower precision are difficulty in determining the onset of shear motion because of wave dispersion, closeness in the gage locations, and errors in gage fabrication.

The shear wave data obtained in this work represent the first such measurements in an elastomer. These data are also unique in that they provide a direct measure of the shear modulus at high strain rates and with increasing pressure. As indicated earlier, ultrasonic measurements of shear wave velocities in elastomers have generally not been successful.

The multiple gage data presented have been used to obtain the dynamic shear stress-strain relations given in Section 4.

The data presented in Figures 3.2 through 3.4 show that the perturbation due to the longitudinal wave is quite small. To more rigorously examine this perturbation, particularly at late times, we performed a uniaxial strain[*] experiment (Experiment 6 in Table IV) and monitored the shear wave signal. Two gages were used (at 1 and 2 mm depth into the sample); the target assembly used for this experiment is shown in Figure 2.2.

---

[*] θ = 0 in Figure 2.1.

The results of this experiment are shown in Figure 3.5, with a vertical scale 2.5 times more sensitive than that in Figure 3.4. Over the useful recording time (6-7 μs after impact) of the experiment, the shear wave signal is nearly zero, as expected. These data confirm the validity of our experimental method. The minor derivations that do occur are caused by several factors: imperfect alignment of magnetic field, impact misalignment, and errors in fabricating gages.

3.3 Tension Results
3.3.1 Plain Solithane

The results of the plain Solithane experiments are summarized in Table V. In all of these experiments, the flyer plates were also made of plain Solithane. The compressive stresses and tensile duration values provide only a qualitative estimate of the magnitude and duration of the tensile pulse because of reasons discussed in Section 2. The exact determination of the tensile pulse magnitude and duration requires a computational analysis incorporating nonlinear moduli and the effects of growing damage (i.e., stress relaxation).

The recovered specimens are cut along a diameter and examined using optical or scanning electron microscopy. Representative results, from Experiments 1 and 2, are shown in Figure 3.6. An increase in damage with increasing impact velocity can be observed. Experiments 4 through 7 were designed for pull-back signal measurements and not for recovery of specimens. However, these specimens were also recovered with minimal ancillary damage. The specimen from Experiment 4 including the gage, is shown in Figure 3.7. Visual examination revealed comparable damage in specimens from experiments 3 and 4. The internal cracking observed in experiment 3 is shown at a higher magnification in Figure 3.8. The localized nature of the damage and the relatively clean separation of the crack surfaces can be seen.*

---

* We caution the readers about sample preparation for microscopic examinations. The pictures shown in Figure 3.6 are for samples that were cut with a razor blade and then lapped and polished. The scanning microscope observations at higher observations revealed considerable amount of fine particles at the crack surfaces. This observation, suggesting large surface area production, was an experimental artifact due to the polishing. The pictures in Figure 3.8 are from a cut, unlapped sample and more truly represent the actual damage.

31
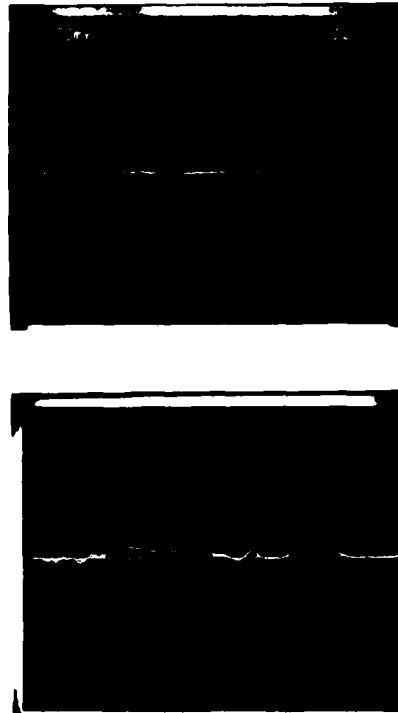
JP-7802-8

FIGURE 3.5   RESULTS OF THE NULL EXPERIMENT (COMPRESSIVE STRESS = 12.0 kbar)

Shear wave signal from a uniaxial strain experiment (80-2-59). The resulting
voltage is nearly zero, as expected. Note, the voltage scale is 2.5 times more
sensitive than the last figure.

Table V

SUMMARY OF PLAIN SOLITHANE EXPERIMENTS[a]

Experiment No.	Impact Vel. (mm/μs)	Flyer Thickness (mm)	Specimen Thickness (mm)	Compressive Stress[b] (kbar)	Tensile Duration[c] (μs)	Comments
1 (79-2-11)	0.052	4.1	7.8	0.43	4	Minimal damage
2 (79-2-12)	0.089	4.3	8.4	0.80	4	Internal cracking
3 (79-2-13)	0.166	3.8	9.1	1.62	4	Internal cracking
4 (80-2-61)	0.164	4.4	9.6	1.60	4.3	Internal cracking[d]
5 (80-2-55)	0.168	4.4	6.73	1.65	2.2	Internal cracking[d]
6 (80-2-49)	0.170	4.4	9.38	1.66	4.3	Internal cracking[d]
7 (80-2-53)	0.249	4.4	9.27	2.6	4	Internal spall[d,e]

[a]In all experiments the flyer plates were also plain Solithane.

[b]This stress is determined from the σ-u relation for plain Solithane.

[c]This tensile duration is valid only when there is no tensile damage.

[d]Samples used for pull-back signal experiments.

[e]This sample was completely spalled except at the ends.

33

(a)

(b)

JP-7802-9

FIGURE 3.6   SPECIMEN DAMAGE IN TENSILE RECOVERY EXPERIMENTS

(a) Experiment 79-2-11, impact velocity = 0.052 mm/μs;
(b) Experiment 79-2-12, impact velocity = 0.089 mm/μs.
The samples are approximately 8 mm thick.
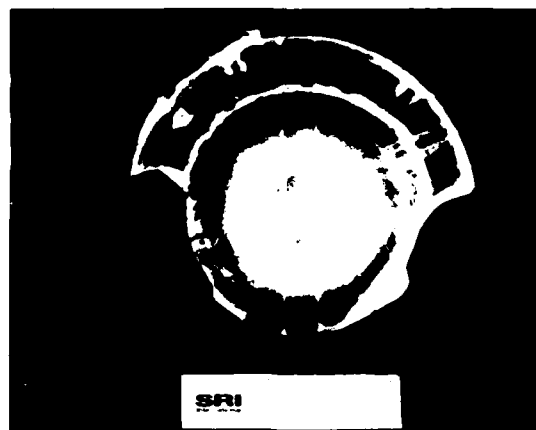
(a)

(b)

JP-7802-10

FIGURE 3.7   SPECIMEN RECOVERED FROM A PULL-BACK EXPERIMENT

(a) Top view;   (b) Side view showing location of damage.

35
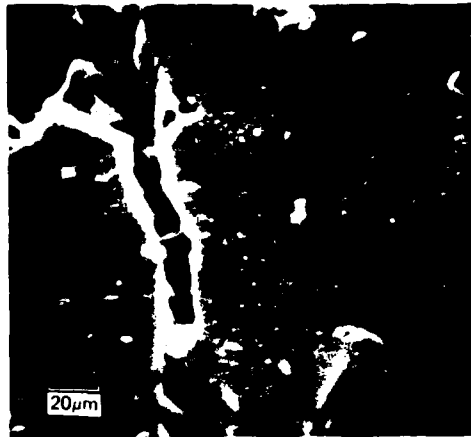
(a)
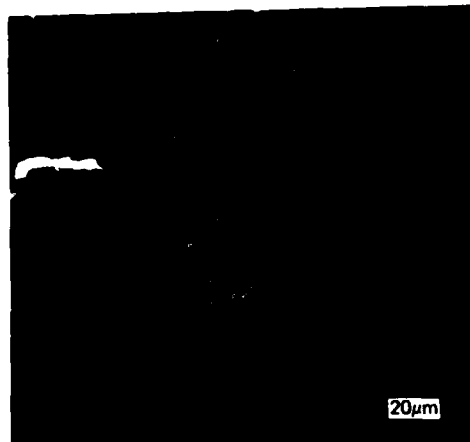
(b)

JP-7802-11

FIGURE 3.8 SCANNING MICROSCOPE PICTURES OF A TENSILE CRACK

The pictures are from Experiment 79-2-13. The localized nature
of the damage can be seen.

36

Experiment 7, conducted at a higher impact velocity, showed macro-
scopic spallation. A scanning microscope picture showing the internal
surfaces is presented in Figure 3.9, which also gives some indication
of the surface roughness due to dynamic fracture. The main features of
the tensile damage observations are summarized below:

(1) The damage location occurs fairly close to the
    region predicted by simple wave interaction.

(2) The damage is very localized.

(3) The flyer plates, which are subject only to compression
    in the propagation direction, show no tensile damage
    and demonstrate the adequacy of the experimental method.

(4) It is difficult to quantify the damage by counting
    individual cracks as was done for metals.[30]

The above observations suggest an elastic-brittle response for the plain
Solithane. To quantify the damage, we attempted to monitor the sample
thickness before and after impact. However, the extremely compliant
nature of the specimens gave ambiguous results. Our reasons for not
attempting the surface area and the volume porosity measurements for
plain Solithane samples are explained in the discussion on filled
Solithane samples (3.3.2).

To quantify the tensile damage and to obtain data on the microsecond
time scales, we attempted the pull-back signal measurements. The results
have been very encouraging, but not completely successful. The difficulty
is in ensuring the survival of gage leads; we have had success in three
of the six experiments we have attempted. The results of these experi-
ments (5,6, and 7) are shown in Figure 3.10. Because the gages are not
exactly at the free surface, we expect to see a two-step jump to the peak
amplitude. In experiment 6 (80-2-49), this was observed. In the other
experiments, impact tilt was apparently too high to see a clear two-step
wave. However, a break in the slope can be seen. The peak amplitude
measured for experiments 5 (80-2-55) and 6 (80-2-49) was lower by about
4 to 6 percent than the correct value. In contrast, the peak amplitude
was higher by about 10 percent in experiment 7 (80-2-53). These results
show that our experimental technique needs to be improved.

37

JP-7802-12

0.5 mm

FIGURE 3.9 CRACK SURFACES FROM A SPALL EXPERIMENT (80-2-53)
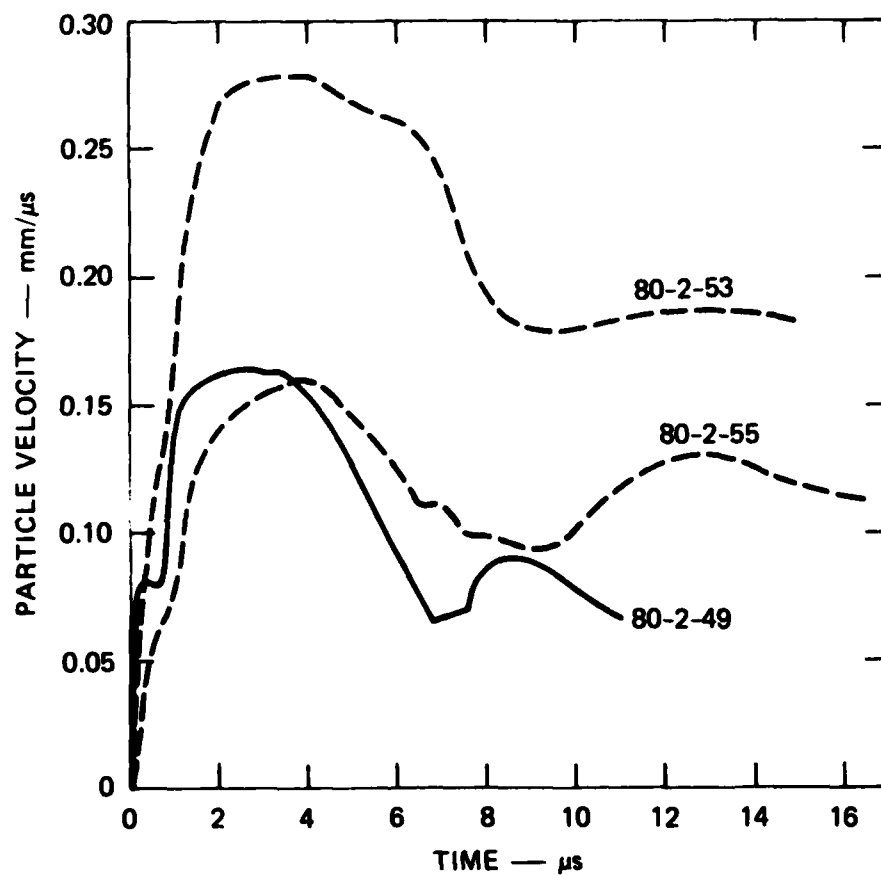
JA-7802-13

FIGURE 3.10   PARTICLE VELOCITY TIME PROFILES FROM PULL-BACK
SIGNAL EXPERIMENTS

The overall shape of the records is qualitatively as expected for a time-dependent fracture process. The hypothetical record shown in Figure 2.4 is similar to the actual data. The first drop from the peak amplitude is a measure of the dynamic tensile strength. For the three records shown in Figure 3.10, we estimate a change in particle velocity of about 0.9 ± 0.2 mm/μs. Using the velocity of the middle point of this jump, this drop in particle velocity corresponds to a stress of 0.75 kbar.[*] This value is higher than the stress level at which the lowest damage is observed in the recovery experiments. However, this comparison is not completely valid because in one experiment we are looking at the equilibrium stress value causing damage, whereas in the other experiment we are looking at an instantaneous stress value.

All three experiments in Figure 3.10 show the recompression signal, but more detailed analysis and/or further comparison between the records are precluded by the quality of the data at late times. In summary, the pull-back signal measurements appear to be promising in quantifying tensile damage in elastomeric materials. However, more experimental developments (specifically, gage emplacement) are needed for obtaining better data. This information will be a valuable complement to the recovery experiments, which provide a description of the damage morphology.

3.3.2 Filled Solithane

The results of the filled Solithane experiments using flyer plates of the same material are summarized in Table VI. The remarks about tensile stress magnitude and duration presented earlier are again applicable. Figure 3.11 shows a picture of the sectioned samples (razor blade cuts) from experiments 3 (79-2-35) and 6 (79-2-38). The tensile damage occurred at locations expected from simple wave interaction analysis. The damage from the same two experiments are shown at higher magnifications in Figures 3.12 and 3.13. These figures again show the localized nature of the damage. No individual cracks are seen; instead, one continuous crack

---

[*]A more rigorous method will be used to determine the stress with better data.

Table VI

SUMMARY OF FILLED SOLITHANE EXPERIMENTS[a]

Experiment No.	Impact Vel. (mm/µs)	Flyer Thickness (mm)	Specimen Thickness (mm)	Compressive Stress[b] (kbar)	Tensile Duration[c] (µs)	Comments
1 (79-2-26)	0.101	3.89	7.82	1.55	4	Damage barely visible
2 (79-2-28)	0.105	3.89	7.49	1.65	4	Very minimal damage
3 (79-2-35)	0.122	3.48	6.99	1.90	4	Extensive internal cracking
4 (79-2-27)	0.139	3.89	7.60	2.18	4	Complete spall
5 (79-2-37)	0.127	8.43	9.28	2	0.8	No damage
6 (79-2-38)	0.266	7.21	8.13	4.6	0.8	Considerable internal cracking

[a]In all these experiments the flyer plate was also filled Solithane.

[b]This stress was determined from the σ-u relation for filled Solithane.

[c]This tensile duration is only valid when there is no tensile damage.

41
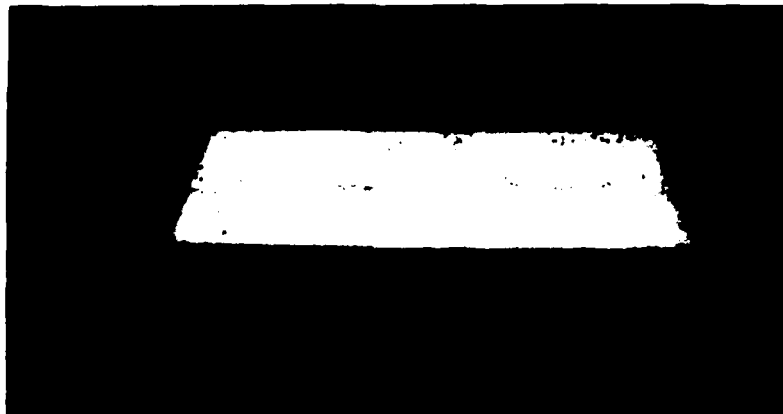
(a)
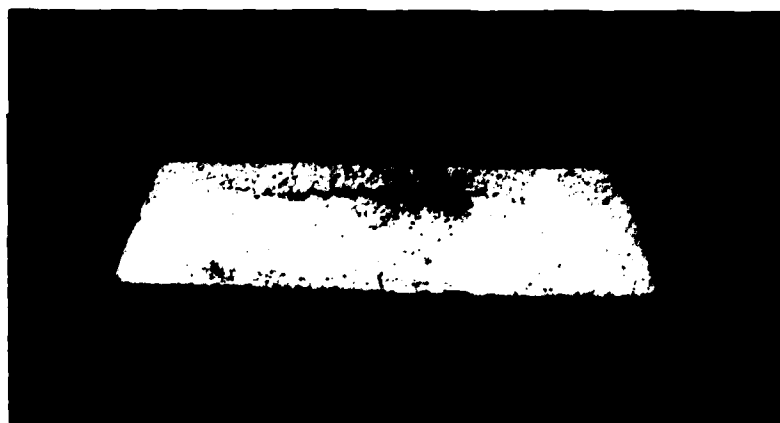
(b)

JP-7802-14

FIGURE 3.11   TENSILE DAMAGE IN FILLED SOLITHANE SAMPLES

(a) Experiment 79-2-35, sample thickness = 7 mm;
(b) Experiment 79-2-38, sample thickness = 8.1 mm.

42
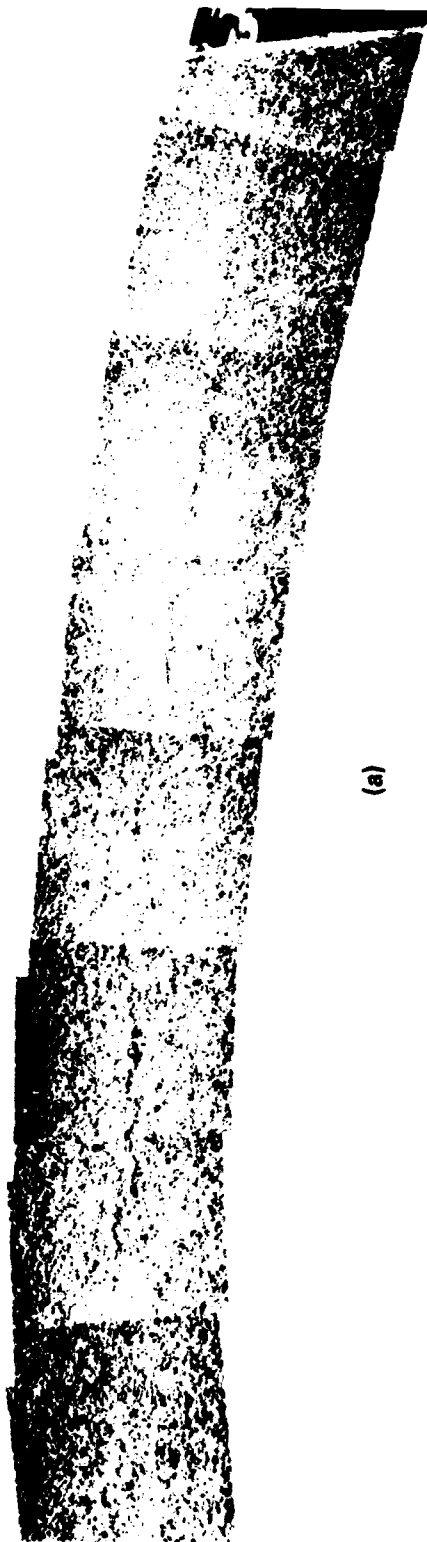
(a)
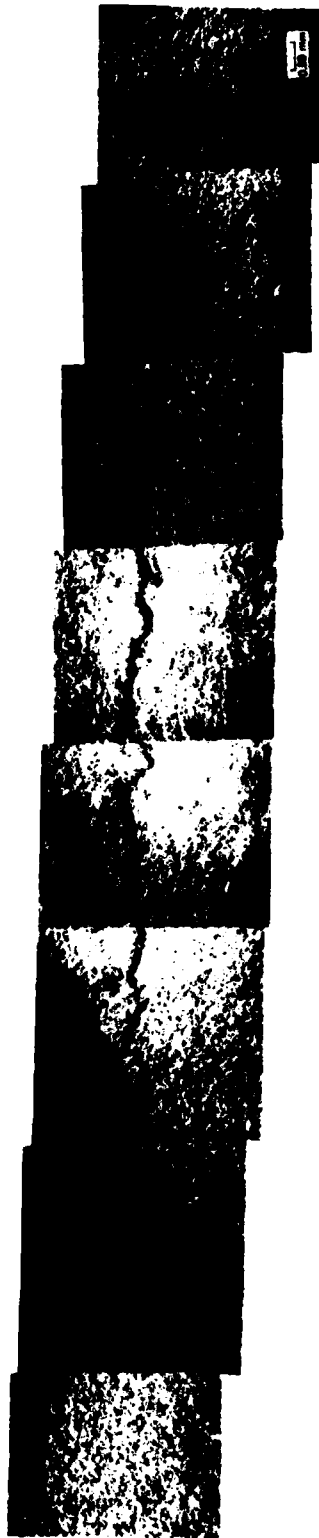
(b)

JP-7802-15

FIGURE 3.12 HIGHER MAGNIFICATION PICTURES OF SAMPLES SHOWN IN PREVIOUS FIGURE (3.11)

The localized nature of the damage can be seen (a) Experiment 79-2-35; (b) Experiment 79-2-38.

43
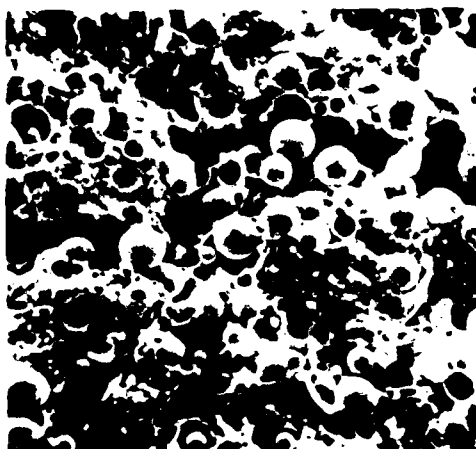
(a)
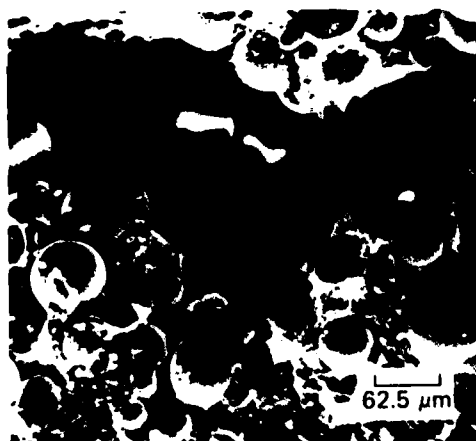
(b)

JP-7802-16

FIGURE 3.13   SCANNING MICROSCOPE PICTURES OF TENSILE DAMAGE
IN FILLED SOLITHANE

(a) Experiment 79-2-35; (b) Experiment 79-2-38. The debonding
between the beads and the matrix, and the matrix fracture can be
observed.

44

can be observed. This observation suggests that cracks nucleate very close to each other (most likely at filler particles) and are joined very quickly.

The high magnification pictures show further details of the tensile damage and several observations can be made. The fractures consist of filler-matrix debonding and matrix fracture. Examination of the regions away from the fracture show that adhesion between the matrix and the filler is generally poor. There appears to be more debris than in the plain Solithane specimens. Because of the elastomer-filler debonding, the fractured surfaces are rougher and are expected to result in a higher surface area. A quantitative determination of the damage from these data is again not possible.

The results in Table VI clearly show the increase in damage with both the impact velocity and pulse duration. Increasing the impact velocity from 0.1 to 0.14 mm/μs changes the specimen response from no damage to complete spall. Increasing the pulse duration (compare experiments 3 and 4 with 5) has the same effect. This transition from no damage to complete spall is sharper than that observed in plain Solithane, suggesting a more brittle response (a lower strain to failure). We caution the reader about comparing the stress threshold for damage for plain and filled Solithane using the compressive stress values cited in Tables V and VI. Without a constitutive model, it is difficult to determine the tensile stresses corresponding to the compressive stresses (particularly for filled Solithane). Finally, comparisons between plain and filled Solithane are most appropriate when there is good bonding between the matrix and filler particles. This was not the case in the present work.

We attempted to quantify the damage by measuring volume porosity using a Mercury porosimeter. The data showed good correlation with the visual observations. However, more careful examination of the data and the samples showed that the Mercury was not being forced into the pores. Instead, we were most likely measuring the compressibility of the samples usng the pressurized Mercury. Therefore, the samples with the higher damage were more compressible. Because this difficulty is increased with the more compliant plain Solithane samples, no measurements were made on plain Solithane.

45

The BET method is commonly used to determine the surface area of specimens. To determine if this method could be used to quantify the fracture damage, we sent four samples* (two unshocked and two shocked) to the Materials Analysis Laboratory of the Micromeritics Instrument Corporation.[37] The measurements were made with the multipoint BET method using Krypton adsorption. The results are presented in Table VII.

Table VII

SUMMARY OF BET MEASUREMENTS

Sample Identification	Experiment No.	Specific Surface Area (m^2/g)	
		Trial 1	Trial 2
1	Control	0.013	0.018
2	Control	0.015	0.023
3	79-2-34	0.043	0.023
4	79-2-38	0.046	0.028

The results of the first trial were very encouraging and showed large differences between the control and the damaged specimens. (Perhaps we should have stopped at this stage.) However, the second trial gave entirely different precision. Our discussions with the laboratory personnel indicate that the lack of precision is most likely caused by the small size of the sample. For accurate results, the samples need to be large enough to provide a surface area of 0.1 m^2/g. In future measurements, we will send either bigger samples or more pieces. In summary, the BET method looks promising, but we have not demonstrated it to be entirely satisfactory.

---

*Cylindrical pieces were cored out of the impacted samples to fit the size of the measuring apparatus.

Section 4

ANALYSIS AND DISCUSSION

The results presented in Section 3 have been analyzed to determine
the dynamic moduli and the stress-strain relations needed for developing
a constitutive model. For plain Solithane, comparisons with other data
are also presented. The wave profiles obtained from the impact data
were analyzed using the Lagrangian Analysis for Compression and Shear
Waves.[38] This method, which is an extension of the method developed
for compression waves,[39] is briefly discussed in Appendix B.

4.1 Compression Data

We start with the compression profiles because these data specify
the density in the shocked state and hence provide a reference for all
the impact experiments. The wave profiles shown in Figure 3.1 were
analyzed to determine the compressive stress-volume (σ_x - V) loading and
unloading path shown in Figure 4.1. Because of the nearly steady nature
of the compression wave, the peak stress-volume state is close to the
state obtained using the Rankine-Hugoniot jump conditions.[40]

Loading and unloading paths, similar to that in Figure 4.1, were
obtained for the other compression experiments, and the peak stress-
volume data from these experiments for plain and filled Solithane are
shown in Figure 4.2. The experimental data were fitted using the following
relations:

Plain Solithane: $\quad \sigma_x = 30\mu + 132.1\mu^2 + 525.5\mu^3$ kbar $\qquad$ (4.1)

Filled Solithane: $\quad \sigma_x = 49.02\mu + 415.9\mu^2 - 639.2\mu^3$ kbar $\qquad$ (4.2)

In fitting the plain Solithane data, we matched the first term to the
ultrasonically determined modulus at ambient pressure. To better define

47

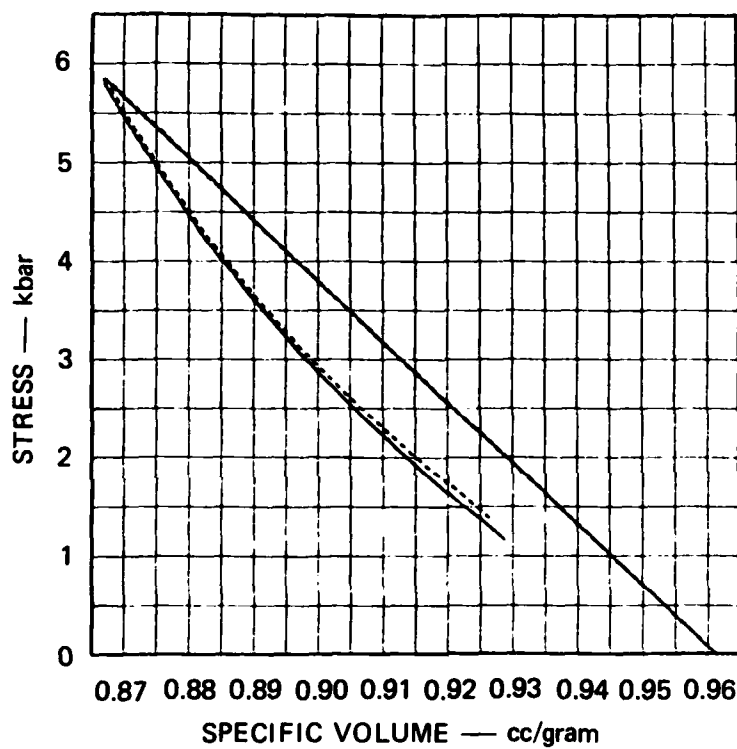JA-7802-17

FIGURE 4.1   LOADING AND UNLOADING PATH FOR A COMPRESSION EXPERIMENT
(80-2-33)
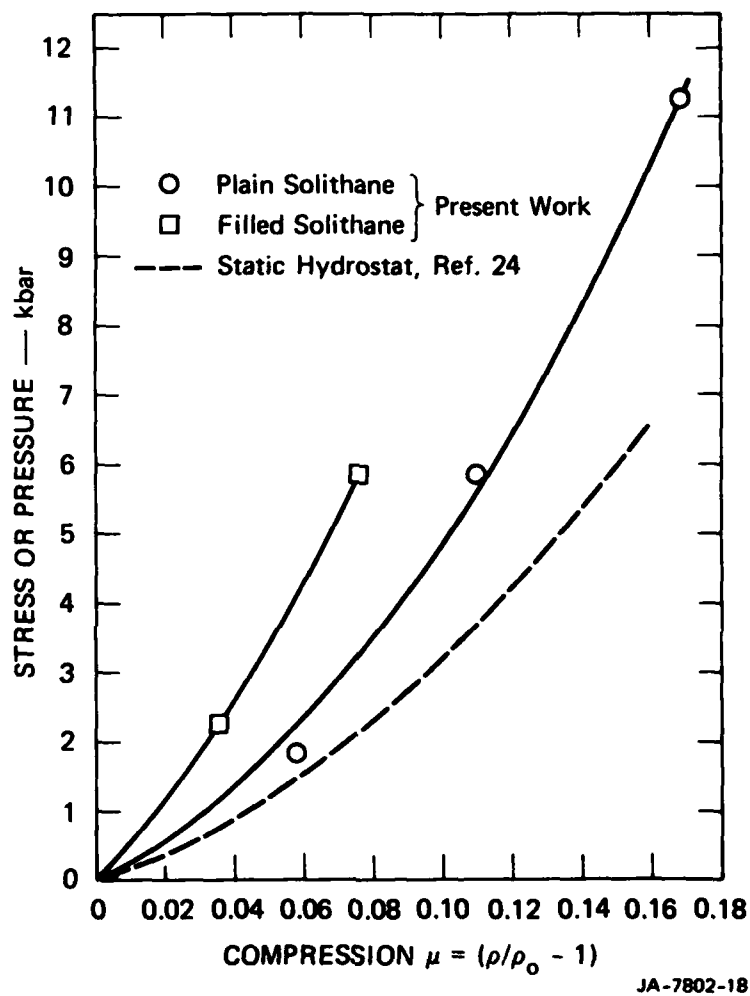
The data from all the gages can nearly be superimposed.

FIGURE 4.2 COMPRESSIVE STRESS-VOLUME DATA FOR PLAIN
AND FILLED SOLITHANE

The solid lines are smooth curves drawn through the data.
The static hydrostat from Ref. 24 is also shown for
comparison. See text comments regarding data at low
stresses.

49

the curve in the lower stress region, we need more data points.* For filled Solithane, the first term is very close to the longitudinal modulus determined from ultrasonic measurements. We have also shown the static hydrostat for plain Solithane from the work of Questad et al.[24] In Appendix C, we have tabulated their data, along with the bulk and shear moduli reported in their paper.

The differences in the impact stress data and the static hydrostat for a given compression for plain Solithane are primarily due to the frequency or strain-rate dependence of the bulk modulus and are not related to material strength. This hypothesis is confirmed by the extremely low shear modulus for plain Solithane discussed in the next subsection. Therefore, the curves in Figure 4.2 are a good approximation to the dynamic mean stress-volume curves for plain Solithane. In shock wave studies of inorganic crystals and metals, the difference in the shock stress and the hydrostat is commonly attributed mainly to the material strength.[40] Our results demonstrate clearly that this assumption can lead to significant error.

Table VIII summarizes data for the shocked state for ten compression and shear experiments. The procedure for determining the cited values of particle velocity, stress, and density change is as follows. First, the $\sigma_x - \mu$ curves shown in Figure 4.2 are used in conjunction with the jump conditions[40] to obtain the stress-particle velocity ($\sigma_x - u$) curves. Then, using an impedance matching method, we employ the $\sigma_x - u$ curves for Solithane and the impactor materials to determine the σ_x, u, and ρ/ρ_o values for all the experiments.† If our procedure is completely error-free, then the values for the three compression experiments should be identical to the values obtained by directly analyzing the experiments. We have obtained a systematic error of approximately 5 per cent in all three experiments. In every case, the values computed using the impedance

_____

*The difference in the low stress datum and the fitted curve is higher than indicated by our precision estimates. We plan to repeat this measurement.

†This procedure was also used to give the compressive stress values cited in the tension results in Section 3.

Table VIII

CHARACTERIZATION OF THE SHOCKED STATE

Experiment Identification	Longitudinal Particle Vel. (mm/µs)	Longitudinal Stress (kbar)	ρ/ρ_o	Wave Velocities in the Shocked State Corrected for Compression	
				Longitudinal (mm/µs)	Shear (mm/µs)
80-2-34 (C, P.S.)	0.104	2.1	1.055	1.98	--
80-2-33 (C. P.S.)	0.247	6.05	1.116	2.87	--
80-2-35 (C, P.S.)	0.411	11.9	1.173	3.35	--
80-2-48 (S, P.S.)	0.106	2.15	1.055	--	0.56
80-2-46 (S, P.S.)	0.248	6.1	1.116	--	0.61
80-2-65 (S, P.S.)	0.247	6.1	1.116	--	0.55
80-2-51 (S, P.S.)	0.413	12.0	1.174	--	0.81
80-2-66 (S, P.S.)	0.470	14.3	1.191	--	0.78
79-2-41 (C, F.S.)	0.072	2.25	1.036	2.36	--
79-2-42	0.165	5.9	1.076	2.88	--

[a]The shot numbers relate to Tables II and III; C and S refer to compression and shear experiments; respectively; P.S. and F.S. refer to plain and filled Solithane, respectively.

match method were higher. Given the precision of our data, the few data points, and the uncertainty in impactor data, these errors are reasonable. To be consistent with the other experiments (where the compression wave profiles were not measured), we have used the impedance matching method values in all cases, and these are cited in Table VIII.

From a knowledge of the Hugoniot (we have used this term in an approximate sense) data of the constituents, we can estimate the Hugoniot for the mixture. McQueen et al., have reviewed several theoretical formulations used for predicting the mixture response.[41] We have used the simplest procedure: The specific volume of the mixture is given by

$$V_m = \sum_i f_i \, V_i \tag{4.3}$$

where f_i and V_i are the mass fraction and the specific volume of the ith component. This procedure ignores the differences in particle velocity and temperature change for the two constituents. The work by Hopkins[41] suggests that for low stresses (comparable to our experiments), this procedure is reasonable. In our calculations, we have approximated the response of the glass beads using Keough's data on soda lime glass[42] (ρ_o = 2.49 g/cm^3) to estimate the response of the filled Solithane. The calculated results are compared with the experimental data in Figure 4.3; clearly, the results are quite good.

4.2 Wave Velocities

Table VIII shows the longitudinal and shear wave velocities in the shocked state. These values were obtained from the measured values C_m by correcting for the compression

$$C = (\rho_o/\rho_o) \, C_m$$

The corrected values are assumed to be related to the longitudinal and shear modulus as follows:[18]

$$C_{LH} = [(K_H + 4/3 \, G_H)/\rho]^{1/2} \tag{4.4}$$

$$C_{SH} = (G_H/\rho)^{1/2} \tag{4.5}$$
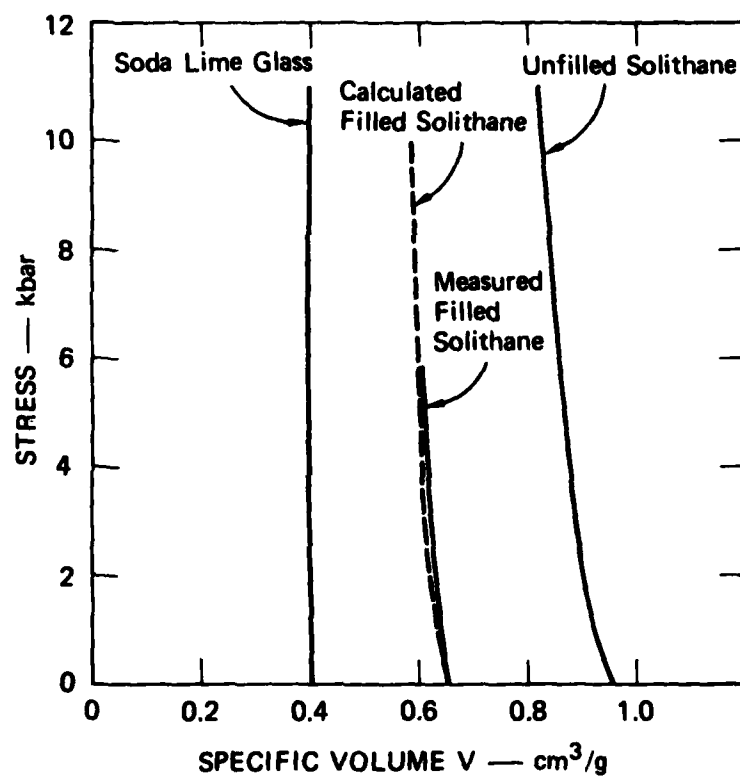
JA-7802-19

FIGURE 4.3 CALCULATED AND MEASURED STRESS-VOLUME CURVE
FOR FILLED SOLITHANE

The measured curves for glass are from Ref. 42.

53

where K and G are the bulk and shear modulus, respectively. The subscript H defines the compressed state obtained by shock loading.

In Figure 4.4, the longitudinal modulus is plotted as a function of compression and compared with very high frequency (10^{10} Hz),[43] ultrasonic (10^6 Hz), and quasi-static measurements.[24] These three sets of data were measured as a function of pressure and we have used the hydrostatic curve of Questad et al.[24] to obtain the corresponding density compression. As shown , the modulus increases with frequency. The shock and ultrasonic data, because of comparable frequencies, are closer. However, the longitudinal moduli determined from the shock data do not vary in a smooth manner. The longitudinal modulus value at a compression of $\mu = 0.058$ appears to be low. We plan to repeat this experiment to verify this result. If this value is indeed low, then we can also change the $\sigma - \mu$ (Eq. 4.1) relation to match the experimental data more accurately. Unlike the three curves shown in Figure 4.4, the shock data are for adiabatic conditions. Hence, the effects of temperature (expected to be small at these stresses) are integrated into the shock data.

In Figure 4.5, the shear velocity and moduli from the impact experiments are plotted as a function of density change and compared with the statically measured shear moduli from the work of Questad et al.[24] The error estimates in the shock data are indicated; the reasons for these errors were discussed in Section 3.

The dynamic and static shear modulus values not only are quite different, but also show markedly different trends. Questad et al.[24] report a pressure-induced glass transition at room temperature that is accompanied by a change of more than two orders of magnitude in the Young's modulus. No abrupt changes were observed in the bulk modulus. The lowest static datum indicates the compression corresponding to this glass transition. Below this compression value, the shear modulus is too low to be plotted in Figure 4.5. In the glassy state, the shear modulus increases with pressure, but appears to be reaching a constant value. The impact data, on the other hand, start out nearly constant, but indicate a sharp increase with compression at larger pressures. These differences in the two sets of data reflect the rate dependence of shear moduli; this dependence needs to be included in constitutive models for intermediate strain rates.

54
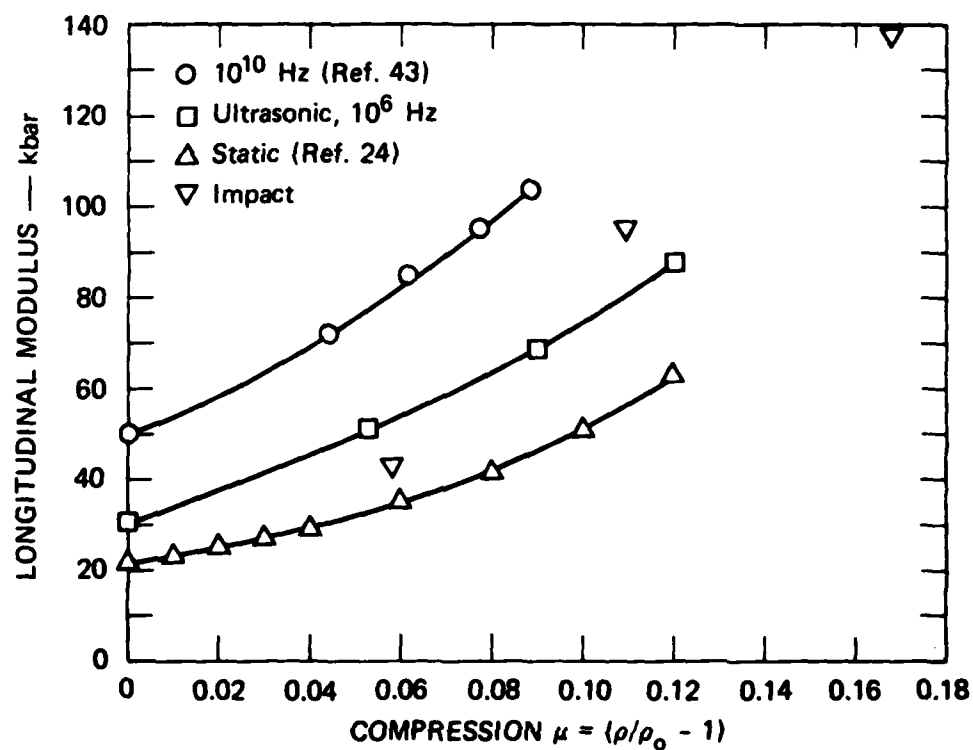
FIGURE 4.4 LONGITUDINAL MODULUS-COMPRESSION DATA FOR PLAIN SOLITHANE
See discussion in the text about ultrasonic and impact data.
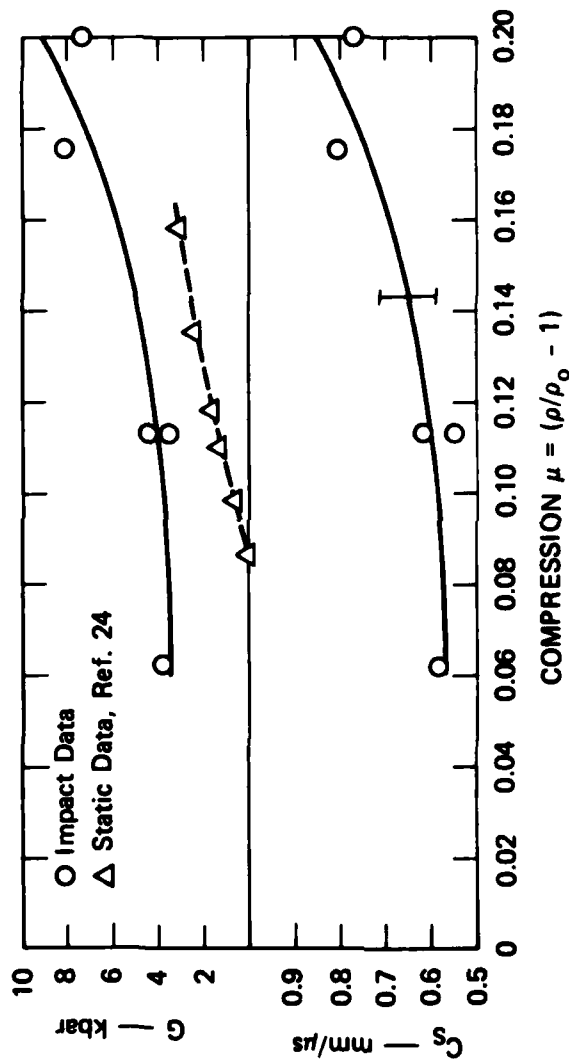
JA-7802-20

55

FIGURE 4.5 SHEAR VELOCITY AND MODULUS AS A FUNCTION
OF COMPRESSION IN PLAIN SOLITHANE

The error bar is an estimate of the experimental precision.
The static data from Ref. 24 are also shown.

JA-7802-21

56

The sharp increase in the dynamic data is in contrast to the data on PMMA[18] and suggests that temperature increase due to compression may not be very large or may have lesser influence than the pressure-induced increase. The shear modulus increase with compression cannot continue indefinitely, and it would be desirable to determine the compression level where the shear modulus levels off (glassy state) or even drops as a result of temperature effects. A knowledge of this compression threshold would also be useful for clarifying the role of localized shear deformations at high strain rates.

Despite the glassy response of the Solithane, the shear moduli in Figure 4.4 are lower than the static values for PMMA ($\sim$10 kbar) and considerably lower than the dynamic values (>20 kbar).

The low shear modulus values demonstrate that the σ_x - μ curves for plain Solithane in Figure 4.2 can be identified with high strain-rate mean stress-volume compression ($\sigma_{mm}/3 - \mu$) to a good approximation. Because many of the applications involving elastomers span a range of strain rates, the rate dependence of the bulk modulus seen in Figure 4.2 *must be included in the constitutive response.*

4.3 Dynamic Shear Response

One of the main objectives of our work was to determine the dynamic shear stress-strain response of elastomers. We have been successful in meeting this objective. The shear wave profiles presented in Section 3 were analyzed using the Lagrangian analysis for shear waves. We analyzed the three experiments that gave the best data (80-2-48, 80-2-46, and 80-2-66) and also covered the maximum range of compression. The resulting stress-strain curves are presented in Figure 4.6. Several features are noteworthy: (1) a decreasing modulus with increasing strain can be seen for all of the experiments, (2) the stress-strain curves are similar to that of an elastic-plastic solid with the yield stress correspondng to a strain of approximately 0.025,[44] (3) the initial modulus and the yield stress increase with compression, and (4) these data are generally similar to quasi-static torsion data on glassy polymers.[19]
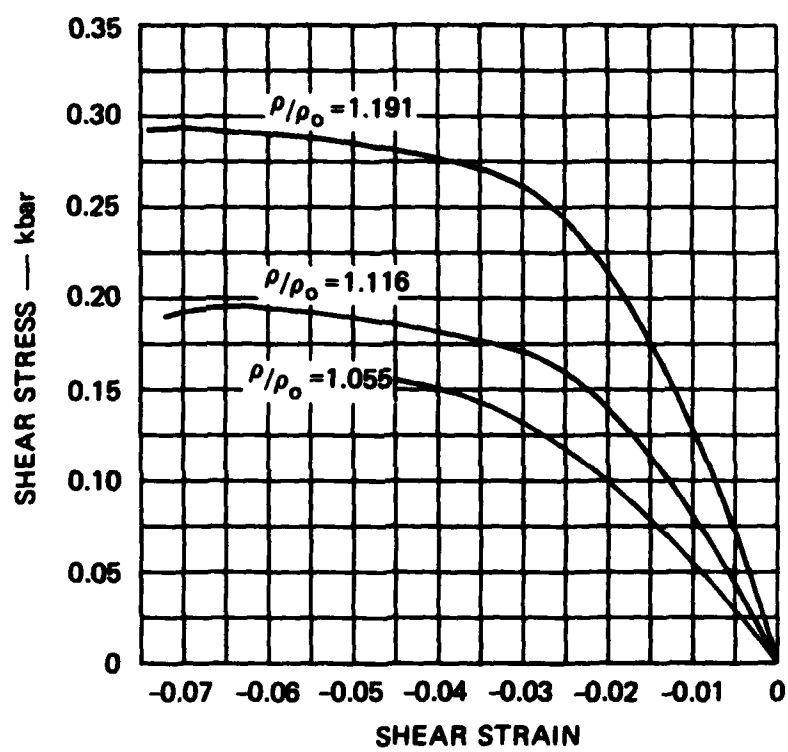
FIGURE 4.6   DYNAMIC SHEAR STRESS-STRAIN RESPONSE
AT DIFFERENT COMPRESSIONS

58

We cannot directly compare our data with data from other studies because the present data are the first of their kind. We will, however, make some comparisons with the quasi-static and impact data on PMMA. Quasi-static torsion measurements under pressure have been reported by Rabinowitz et al.[19] The overall data are similar to ours. However, the initial moduli and the yield point are considerably higher than the Solithane values. This result suggests that even at high strain rates, the Solithane is not approaching the stiffness of PMMA.*

Comparisons with the impact data on PMMA provide interesting results. In a separate study we have examined the high strain-rate response to PMMA using compression and shear wave velocity measurements.[18] These data showed that up to 8-kbar compressive stress, PMMA responds as a nonlinear elastic solid. Large amplitude shear waves could be propagated below this stress level. Above 8 kbar, however, there is an apparent loss of strength and it was difficult to propagate large amplitude shear waves with increasing compression. This result is in marked contrast to our Solithane results shown in Figure 4.6. Because of the PMMA work, we believe that the strength increase observed in Figure 4.6 cannot continue indefinitely for higher compressions.

The data reported in Figure 4.6 are expected to be important for applications where the dynamic shear properties of the elastomers are required. As indicated in Section 4.1, it is impossible to infer much information about the shear response by examining the compression data as is frequently done for inorganic solids.

---

*Despite our remarks here, comparisons between quasi-static and shock data must be viewed with caution because of differences in the two states. The main difference is that quasi-static data are isothermal, whereas the shock data are adiabatic. This transition from isothermal to adiabatic conditions can dominate the material response.

In our discussion so far, we have not indicated the accuracy of our Lagrangian analysis in determining the stress-strain response from particle velocity curves. The analysis procedure has been discussed for uniaxial strain (compression only) in previous SRI work[39] and for shear wave profiles in a separate report[38] and we make the following observation: The integration of the governing equations using the particle velocities is satisfactory when there are three or more gages and no significant attenuation is observed. This condition was met in our compression profiles. For shear wave profiles, this condition was not fulfilled.[*] It is difficult to evaluate the accuracy in an absolute manner. Instead, we checked our results by inverting the stress-time profiles obtained from the experimental values of the particle-velocity profiles. The particle velocity profiles obtained by this reanalysis compared very well with the original data. There is some ambiguity about rate effects for the highest compression level.[†] More discussion on this particular subject is presented in Reference 45 and will be addressed in future reports when more data from three or four gage profiles are available in shear wave experiments. It would also be desirable to use the results in Figure 4.6 in a wave propagation code to calculate shear wave profiles and to compare them with experimentally measured profiles.

4.4 Tension Results

In our experiments both the plain and filled Solithane materials exhibited an elastic-brittle response. However, the filled Solithane specimens showed a sharper threshold between no damage and complete spall in contrast to the plain Solithane specimens. This result can be explained by the linking of the cracks nucleated at the filler-elastomer interface. Given the volume fraction of the glass beads, the crack growth required for coalescence is small and the development of a macroscopic spall is quite rapid. Similar observations can be made for the work on propellants and explosives.[16,17] The above-cited result and other differences in the tensile response of plain and filled Solithane (cited in Section 3) suggest that it is difficult to extrapolate information about tensile cracking in filled samples from unfilled samples.

---

[*] The results shown in Figure 4.6 were based on analysis of two gage profiles.
[†] For this experiment we had three gages, but only two were used.

We have not attempted quantitative analysis of the tensile data because of a lack of suitable measurements. Although the SRI-NAG model[30] appears well suited for describing the fracture behavior, quantitative experimental data are needed to derive the material parameters and then check the model predictions (e.g., comparison with BET measurements). We plan to continue our efforts to make improved pull-back signal measurements and surface area measurements.

Finally, the recent work of Knollman et al.[45] on quasi-static fracture (compression, shear, and tension) of filled elastomers may be relevant to impact studies. These authors have measured the vacuole formation in deformed samples using ultrasonic longitudinal wave measurements. Their data suggest a nucleation and growth mechanism for fracture. For all three loading conditions (compression, shear, and tension), the plane of fracture was normal to the direction of maximum strain. These authors also showed that the principal tensile strain magnitude (measured macroscopically) could be correlated with the volume dilatation measurements. This last observation is useful in developing a tensile fracture model for more general loading conditions (combinations of compression, shear, and tension).

Section 5

SUMMARY

The objectives of the work presented in this report were to directly determine the response of elastomers to compression, shear, and tension under dynamic loading conditions. These objectives have generally been met and a good start has been made in making these measurements. The main results are summarized below.

The compression results in plain Solithane are dominated by the mean stress-volume response. The bulk modulus under impact conditions is considerably higher than that determined from static hydrostatic loading. The response of the filled Solithane is stiffer and to a good approximation can be predicted by a simple mixture theory using the Hugoniots of glass and plain Solithane. The longitudinal modulus measured in impact experiments is similar to ultrasonic values and is bounded by the very high frequency (10^{10} Hz)[43] and quasi-static measurements.[24]

Shear wave profiles have been measured in plain Solithane at several compressions. The wave profiles are dispersive. With increasing compression, the dispersion decreases, but attenuation increases. The shear modulus values range between 3 and 9 kbar for compressive stresses ranging between 2 and 14 kbar. Unlike the quasi-static shear modulus, the dynamic data suggest a rapid increase with compression at higher stresses. High strain-rate, shear stress-strain curves have been obtained at three compression levels. The overall features are similar to quasi-static torsion measurements in glassy polymers under pressure.[19] The stress-strain response is typical of an elastic-plastic solid with yield strength varying between 0.12 kbar and 0.25 kbar for a volume compression ranging from 6 to 20 percent. The compression and shear data can be used to develop a realistic constitutive model at high strain rates.

Tension recovery experiments on plain and filled Solithane show an elastic-brittle response for both materials. The damage is quite localized and the location can be predicted from simple wave interactions. Although the recovery experiments provide a good description of the fracture damage, it is difficult to quantify these experiments. Two types of measurements to quantify tensile fracture were attempted in the present work: (1) pull-back signal measurements to characterize the tensile strength and fracture kinetics on the microsecond time scale, and (2) surface area measurements on recovered specimens using the BET method. Both of these measurements have given encouraging results, but further development is needed before they can be used successfully.

Future work will focus on the following topics:

(1) Measurement of shear response above 15-kbar compression stress.

(2) Measurement of shear response for filled Solithane; we also plan to determine if these measurements can be correlated with the data for plain Solithane.

(3) Attempts to quantify the tensile fracture damage.

(4) Preliminary development of a dynamic constitutive model.

Appendix A

PROCEDURE FOR CASTING SOLITHANE SPECIMENS

The details of casting plain and filled Solithane specimens are described in this appendix. The procedure for casting the plain Solithane is identical to that used at Caltech. Because of the influence of moisture on Solithane, care is taken to transfer and mix the resin "Solithane 113" and the curing agent "C-113-300" under a dry nitrogen atmosphere.

In preparation for casting the plain Solithane samples, the resin and the curing agent are warmed to 50°C. Compressed nitrogen is used to transfer the materials to a mixing chamber. The two components are mechanically mixed under vacuum and at a temperature of 70°C. Dry nitrogen is used to transfer the mixture into heated molds.* The molds are placed in an oven on level shelves to cure at 120°C for 2 hours and the cured samples are slowly cooled to room temperature.

To cast the filled Solithane samples, the following additional steps are included. While the resin is being mixed, the glass beads are weighed, heated, and placed in a mixer that has been heated and filled with nitrogen. The mixed Solithane is then added to the glass beads. The mixture is evacuated to eliminate moisture. Dry nitrogen is forced into the mixer to bring the pressure back to an ambient level. The glass beads and the Solithane are mixed for 10 minutes and then evacuated (25 in. of mercury). The liquid Solithane and glass bead mixture is transferred to the molds using dry nitrogen. The curing process is similar to the procedure used for plain Solithane.

---

*Once the material is transferred into molds, it is no longer under vacuum. Before assembly, all mating parts of the mold are covered with a uniform and very thin layer of vacuum grease.

When the samples are casted for compression and shear experiments, care is taken to hold the gage leads and active elements in their proper position. A Π-shaped fixture is used to hold the thin wires shown in Figure 2.2. This fixture is bolted to a polished ferro-type plate[*] and the whole assembly is placed in a cylinder of appropriate length. After curing, all the components can be disassembled, leaving the gages cast in place. Although the Solithane shrinks on curing, the small length of the active element minimized the gage distortion.

In the pull-back signal experiments, the gage leads must be brought out through the sides. To fabricate the gages, it is necessary to drill through the walls of the cylindrical mold. Wires were carefully stretched and welded (see Figure 3.7) to fabricate and position the gages close to the back surface. After curing, the back surface is ground flat to the appropriate thickness.

---

[*]The surface is sprayed with a thin layer of mold release material like Korac 1711.

Appendix B

GOVERNING EQUATIONS FOR COMPRESSION AND SHEAR WAVE PROPAGATION

This appendix summarizes the equations that govern one-dimensional compression and shear wave propagation. More detailed discussion of these equations and related claculations is given in Reference 29. The notation used here follows that used in the text by Malvern.[*]

In describing the wave propagation for the impact situation shown in Figure 2.1, it is convenient to use the X_1-system. The governing equations are then one-dimensional; that is, variations with respect to only X_1 need to be considered. The current configuration, particle velocity, and deformation gradient are defined, respectively, as

$$x_1 = x_1(X_m, t) \tag{B.1}$$

$$u_1 = \left(\frac{\partial x_1}{\partial t}\right)_{X_m} \tag{B.2}$$

$$F_{ij} = \left(\frac{\partial x_i}{\partial X_j}\right)_t \tag{B.3}$$

With these definitions, we can write the equations governing wave propagation as

$$\rho_o \left(\frac{\partial u_1}{\partial t}\right) = \left(\frac{\partial T_{11}}{\partial X_1}\right) \tag{B.4}$$

$$\rho_o \left(\frac{\partial v}{\partial t}\right) = \left(\frac{\partial u_1}{\partial X_1}\right) \tag{B.5}$$

---

[*] L. E. Malvern, *Introduction to the Mechanics of a Continuous Medium* (Prentice-Hall, Englewood Cliff, 1969).

$$\left(\frac{\partial E_{12}}{\partial t}\right) = 1/2 \left(\frac{\partial u_2}{\partial X_1}\right) \qquad (B.6)$$

$$\rho_o \left(\frac{\partial \epsilon}{\partial t}\right) = T_{1i} \left(\frac{\partial u_i}{\partial X_1}\right) \qquad (B.7)$$

where
T_{1i} = First Piola-Kirchoff stress tensor

ρ_o = initial density

V = specific volume

$E_{ij} = \frac{1}{2} \left(\frac{\partial x_m}{\partial X_i} \frac{\partial x_m}{\partial X_j} - \delta_{ij}\right)$, a finite strain measure

ϵ = specific internal energy.

For the one-dimensional problem under consideration here, the stresses T_{11} and T_{12} are equal to the Cauchy stresses σ_{11} and σ_{12}. While σ_{12} is equal to σ_{21}, T_{12} and T_{21} are not equal. The use of the symbol T in Equation (B.4) emphasizes this difference.

There are seven unknowns in the five governing equations. Hence, a knowledge of u_1 (X_1,t) and $u_2(X_1,t)$ allows us to integrate the above set of equations. The procedure for doing this integration is similar to that used for compression waves[39] and is described in References 29 and 38. We point out two main features of the above equations: (1) no assumptions about the material response are needed to integrate the above set of equations; (2) even in the presence of shear deformation, the specific volume, V, is governed by only u_1.

Appendix C

STATIC DATA ON SOLITHANE

Tabulated below are the pressure, bulk modulus, and shear modulus for Solithane from the data of Questad et al.[24] In addition, we have fitted their pressure-volume data to a third-order polynomial[*] and obtained the density compression corresponding to the pressure.

Hydrostatic Pressure (kbar)	$\mu = P/P_o - 1$[*]	Bulk Modulus (kbar)	Shear Modulus (kbar)
0	0	21.9	0.0074
1.10	0.0440	31.6	0.0088
2.13	0.0745	42.7	0.0111
2.38	0.0815	45.9	0.021
2.57	0.0856	48.1	0.081
2.67	0.0880	49.7	0.156
3.11	0.0978	55.2	0.585
3.67	0.110	60.3	1.35
4.11	0.119	63.5	1.74
5.00	0.135	67.1	2.46
6.50	0.158	81.3	3.01

---

[*] $P = 21.9 \mu + 54.23 \mu^2 + 433.4 \mu^3$ kbar.

REFERENCES

1. G. T. Afans've and V. K. Bobolev, <u>Initiation of Solid Explosive by Impact</u>, Israel Program for Scientific Translations, 1971 (Available from NTIS, U.S. Dept. of Commerce, Springfield, VA).

2. J. Wackerle et al., "Shock Initiation of High Density PETN," in <u>Proceedings of Sixth Symposium (International) on Detonation</u>, 1976 (ACR-221, ONR, Department of the Navy, Arlington, VA).

3. J. F. Kincaid, presentation at the Workshop on "Transition from Deflagration to Detonation," Atlanta, GA (1978).

4. M. S. Chawla and R. Frey, Propellants and Explosives, 3, 119 (1978).

5. S. N. Heavens and J. E. Field, Proc. R. Soc. London, A338,77 (1974).

6. R. E. Winter and J. E. Field, Proc. R. Soc. London A343, 399 (1975).

7. Presentation by M. Finger and R. McGuire at the Workshop on "New Opportunities for Research In Energetic Materials," held at Wrightsville, Beach, NC (1977).

8. A. F. Belyaev et al., <u>Transition From Deflagration to Detonation in Condensed Phases</u>, Chapters III and IV, Israel Program for Scientific Translations, 1975 (Available from NTIS, U.S. Dept. of Commerce, Springfield, VA).

9. W. J. Murri, Y. M. Gupta, and D. R. Curran, "Fracture and Fragmentation of High Energy Propellant," See Appendix, SRI International Final Report to Lawrence Livermore Laboratory, Contract No. 112 under ERDA E(04-3)-115 (1979).

10. The loading conditions of interest for the study of energetic materials span a wide range of strain rates, stresses, and strains. The mechanical response of elastomers at low strain rates is a vast subject and a review of this field is outside the scope of our work. Specific studies pertaining to deformation of rocket propellants may be seen in JANNAF proceedings.

11. Plate impact experiments to study initiation and buildup to detonation are routinely carried out and papers on this subject may be seen in the proceedings of the <u>Sixth Symposium (International) on Detonation</u> (Office of Naval Research, ACR-221); a good account of the empirical tests is given in the report by J. R. Humpherey, "LX-14, A New High-Energy Plastic-Bonded Explosive," Lawrence Livermore Laboratory Report UCRL-52350 (Livermore, CA).

12. <u>J. D. Ferry, Viscoelastic Properties of Polymers</u> (J. Wiley & Sons, Inc., New York, 1970).

13. T. Murayama, _Dynamic Mechanical Analysis of Polymeric Materials_ (Elserier, Amsterdam, 1978).

14. J.W. Nunziato et al., "Wave Propagation in Nonlinear Viscoelastic Solids", in _Handbuch Der Physik_, Volume VIa 14, Ed., S. Flügge (Springer-Verlag, Berlin, 1974)

15. D. R. Curran et al., J. Appl. Phys. 44, 4025 (1973).

16. W. J. Murri and D. R. Curran, "Fracture and Fragmentation of High Energy Propellant," SRI Annual Report to Lawrence Livermore Laboratory, Contract P.O. 7250109 Under W-7405-ENG 48, Menlo Park, CA (November 1980).

17. P. S. DeCarli and Y. M. Gupta, "High Strain Rate Deformation of Composite Explosives," SRI International Final Report to Naval Surface Weapons Center under Contract N60921-79-C-0264 (Menlo Park, CA, 1980).

18. Y. M. Gupta, J. Appl. Phys. 51, 5352 (1980).

19. S. Rabinowitz et al., J. Mater. Sci. 5, 29 (1970); A. A. Silano et al., J. Appl. Phys. 48, 4076 (1977).

20. D. D. Bloomquist and S. A. Sheffield, J. Appl. Phys. 51, 5260 (1980).

21. W. G. Knauss and H. K. Mueller, "The Mechanical Characterization of Solithane 113 in the Swollen and Unswollen State," Calif. Inst. of Technology Technical Report to U.S Air Force Propulsion Laboratory under Contract F-04611-67-C-0057, Pasadena, CA (1967).

22. Glass beads manufactured by Cataphote Division of the Ferro Corporation, P.O. Box 2369, Jackson, MS 39205.

23. Terra Tek, University Research Park, 420 Wakara Way, Salt Lake City, UT 84108.

24. D. L. Questad et al., J. Appl. Phys. 51, 5100 (1980).

25. Discussions with J. Bellin and R. Martinson of Lockheed Research Laboratory, Palo Alto, CA.

26. Craig Tarver, private communication, Lawrence Livermore Laboratory (March 1980).

27. Y. M. Gupta, Appl. Phys. Letters 29, 694 (1974).

28. Y.M. Gupta et al., Rev. Sci. Instr. 51, 183(1980).

29. Y. M. Gupta, "Development of a Technique to Measure Dynamic Shear Properties," Draft Final Report ot the Defense Nuclear Agency under Contract DNA001-76-0384, SRI International, Menlo Park, CA (1978).

30. L. Seaman, J. Appl. Phys. 47, 4814 (1976).

31. S. Lowell, Introduction to Powder Surface Area (John Wiley & Sons, New York, 1979).

32. S. Cochran and D. Banner, J. Appl. Phys. 48, 2729 (1977).

33. D. E. Grady and M. E. Kipp, Int. J. Rock Mech. Min. Sci. & Geomech Abstr. 16, 293 (1979).

34. A particle velocity gage at the free surface works for compression, but does not stay bonded for the release wave from the back of the flyer.

35. L. M. Barker and R. E. Hollenbach, J. Appl. Phys. 41, 4208 (1970).

36. D. B. Larson and G. D. Anderson, Int. J. of Rock Mech. and Min. Sci. 17, 357 (1980).

37. Materials Analysis Laboratory, Micromeritics Instrument Corporation, 5680 Goshen Springs Road, Norcross, GA 30093. This laboratory was suggested to us by Dr. L. Peebles.

38. Y. M. Gupta, "Lagrangian Analysis for Compression and Shear Waves" (manuscript in preparation).

39. L. Seaman, J. Appl. Phys. 45, 4303 (1974).

40. G. E. Duvall, "Shock Waves and Equations of State," in Dynamic Response of Materials to Intense Impulsive Loading, Eds., P. C. Chou and A. K. Hopkins (Wright Patterson AFB, OH, 1972).

41. R. G. McQueen, S. P. Marsh, J. W. Taylor, J. N. Fritz, and W. J. Carter, "The Equation of State of Solids From Shock Wave Studies," in High-Velocity Impact Phenomena, Ed., Ray Kinslow (Academic Press, New York & London, 1970), p. 373.

A. K. Hopkins, "The Dynamic Compression and Release of Mechanical Mixtures in the Presence of a Phase Change," Technical Report AFML-TR-72-264, Air Force Materials Laboratory, Wright-Patterson Air Force Base, Ohio, December 1972.

42. D. D. Keough, "Development of A High-Sensitivity Piezoresistive Shock Transducer For Low Kilobar Range," Final Report For Shock Physics Directorate Defense Atomic Support Agency, Washington, D.C., Contract DASA-69-C-0014, March 25, 1970, p. 28.

43. J. Schnur (private communication, 1980).

44. This definition is comparable to the 2% value used by Silano et al., (Ref. 19).

45. G. C. Knollman et al., J. Appl. Phys. 50, 111 (1979).

73